



Design optimization for a compliant mechanism based on computational intelligence method

Ngoc Le Chau¹ · Ngoc Thoi Tran¹ · Thanh-Phong Dao^{2,3}

Received: 28 June 2020 / Accepted: 7 January 2021 / Published online: 24 January 2021
© The Author(s), under exclusive licence to Springer-Verlag London Ltd. part of Springer Nature 2021

Abstract

Modeling and optimization for compliant mechanisms are challenging tasks thanks to an unclear kinematic merging among rigid and flexible links. Hence, this paper develops a computational intelligence-based method for modeling and optimization. The proposed method concerns about statistics, numerical simulation, computational intelligence, and meta-heuristics. A two degrees of freedom compliant mechanism is investigated to illustrate the effectiveness of the suggested computational intelligence method. First, numerical datasets are collected by simulations. Then, sensitivity of design parameters is analyzed by analysis of variance and Taguchi technique. The results of sensitivity are employed to separate a few populations for lightning attachment procedure optimization (LAPO). Next, the values of two output performances of the mechanism are changed into the values in the range from zero to one through desirability function method. The calculated output values become two inputs of the fuzzy logic model, and the output of this system is a single objective function (SOF). Subsequently, the SOF is modeled by using adaptive neuro-fuzzy inference system (ANFIS). LAPO algorithm is then utilized to maximize the SOF. The results revealed that the numerical example 3 is the best design for the mechanism. In comparison with artificial intelligence techniques and regression, the results show that the performance indexes of the proposed ANFIS model (R^2 close 1, MSE about 10^{-4} , and RMSE about 10^{-2}) are superior to those of the multilayer perceptron, deep neural network, and multiple-linear regression. Additionally, the proposed computational intelligence method is more effective than the Taguchi-fuzzy logic, ANFIS-integrated teaching learning-based optimization, and ANFIS-integrated Jaya in searching the optimal design of the compliant mechanism. The results determined that the optimal displacement and parasitic error are about 2.2109 mm and 0.0028 mm, respectively.

Keywords Modeling · Optimization · Compliant mechanism · Desirability · Fuzzy logic · ANFIS · LAPO · Non-parameter analysis · Artificial intelligence

1 Introduction

Compliant mechanism is a promising platform in accurate positioning engineering. It is widely used across multidisciplinary applications, e.g., micro-electromechanical

system, robotics, bioengineering, actuator, and sensor [1–9]. In recent years, two degrees of freedom (2-DOF) compliant mechanisms have received much attention in industry and academy because they can provide an ultra-high precision and save manufacturing costs. Additionally, they inherit excellent advantages of monolithic fabrication with a lightweight and a friction free compared to conventional counterparts [10–14].

Until now, modeling of the performance for the compliant mechanisms is an extremely complex task due to an incorporation of compliant elements with rigid ones, and a strictly merging of simultaneously kinematic-and-mechanical behaviors. The kinematic methods are mainly based on a relative movement among links and joints, which ignore the simultaneously kinematic-and-

✉ Thanh-Phong Dao
daothanhpung@tdtu.edu.vn

¹ Faculty of Mechanical Engineering, Industrial University of Ho Chi Minh City, Ho Chi Minh City, Vietnam

² Division of Computational Mechatronics, Institute for Computational Science, Ton Duc Thang University, Ho Chi Minh City, Vietnam

³ Faculty of Electrical and Electronics Engineering, Ton Duc Thang University, Ho Chi Minh City, Vietnam

mechanical behaviors. Especially in analyzing a flexible element with largely nonlinear deformation, the applications of kinematic methods are failed. When a flexible element has one more degree of freedoms in movements, the modeling task is more complicated. So, their structures are difficult to analyze and model when they undergo a large nonlinear deformation.

In the last decades, modeling methods for compliant mechanisms have received a great interest by many researchers. Particularly, analytical methods and numerical techniques have been developed such as pseudo-rigid-body model [15], improved pseudo-rigid-body model [16, 17], stiffness matrix [18], kinematic-based methods [4, 19, 20], kineto-static and dynamic model [21], compliance matrix method [22], finite element method (FEM) [23, 24], normalization-based methods [25, 26], nonlinear model [27], and building block [28].

The analytical methods have been successfully applied for modeling simple structures but the state-of-the-art procedures are still challenging due to their complicated applications and even unsolvable for highly nonlinear deformation. Specifically, the pseudo-rigid body model is strongly influenced by assigning the locations of torsional springs and amount of them, and the prediction accuracy is limited. Meanwhile, the compliance matrix method is not capable of analyzing structures with multiple forces.

On the contrary, the FEM method has been successfully employed for analyzing compliant mechanisms due to its efficiency. The FEM can divide each flexible link and rigid into a number of elements and nodes so as to describe a large nonlinear deformation of multiple degree of freedoms compliant mechanisms. The FEM can also analyze complex or irregular shapes. For example, the FEM technique was developed to model the statics and dynamics of circular hinge [29]. And then, this technique was extended for the amplification mechanism with a high accuracy. Additionally, the inverse FEM technique was discovered as a modeling method for compliant mechanism. In this article, microgripper, microvalve, and lens folding devices were illustrated as the irregular shapes or complex structures [30]. The shapes of flexible elements in these devices are irregular curves, and their deformations have very high nonlinearity. For data-based optimization problems in engineering, the FEM is a suitable tool to initialize datasets which are then employed for some tasks such as modeling, prediction, regression, and optimization [31]. So, the FEM is considered as an alternative design method for compliant mechanisms.

In the present work, a computational intelligent method is motivated to solve the compliant mechanisms. The FEM is a key technique which is integrated in the proposed method. The main purpose of the present article is to reach a computation-based intelligent method in modeling and

optimization for compliant mechanisms. The suggested method is based on computational intelligence, statistics, fuzzy logic theory, adaptive neuro-fuzzy inference system, finite element method, and metaheuristic algorithm.

In order to enhance the performances of compliant mechanisms, e.g., fatigue life, displacement, parasitic error, stress, frequency, and strain energy, the mechanical structures are almost changed randomly by designer's experiences. Then, the aforementioned analytical procedures are applied to predict the performances. This improvement process can take a long time and spend a large computing cost. In order to overcome this restriction, researchers have suggested an optimal design method for compliant mechanisms. In the field of optimization, mathematical models of fitness and constraint functions are established, and then a population-based metaheuristic algorithm is applied. Structural optimization is a common type in this field, including topology optimization [32], shape optimization, and size optimization [33–35]. The topology optimization and shape optimization are directly related to FEM and evolutionary algorithm while the size optimization is involved to mathematical models. In the light of this problem, the present study focuses on multi-objective optimization (MOO) via the computational intelligent method. Nowadays, MOO issues have been growing by many researchers [36–38]. Regarding a general MOO, design parameters should be properly chosen to decrease complexity of the problem. Therefore, this article considers an enough amount of design parameters. This work helps to reduce space of populations and make new ones in modeling and optimization process.

Before implementing the optimization problems, fitness functions and constraint objectives must be formulated. In compliant mechanisms, the performances have high nonlinearity. Hence, the objective and constraint functions are difficult to be established through the traditionally analytical methods. In order to overcome this limitation, approximation models are alternated in the present article. Based on the datasets from the FEM simulations, the approximate models can accurately model the performances of compliant mechanisms. In order to reach a global value, data-driven methods are priority. Data-driven methods allow to build regression models or equations such as the response surface method (RSM) [39–41] and Kriging technique [42]. These two methods are still limited because these techniques strongly depend on approximation order, such as linear, second-order, and high polynomial order.

To solve the engineering problems with high nonlinearity behaviors, artificial intelligences (AI) methods or genetic expression programming (GEP) are potential techniques which offer precisely approximate the regression models. Recently, Güllü coupled the AI with genetic expression programming to predict average shear wave

velocity which is soil property [43]. Then, the GEP was developed to forecast the rheological behavior of grout with bottom ash in jet grouting columns [44]. The results of this study show that the performance metrics of the developed model are better than the nonlinear regression models. In order to estimate the nonlinearly rheological characteristics of jet grout cement mixtures, the GEP was applied [45]. Güllü and Fedakar developed AI techniques such as radial basis neural network, multilayer perceptron, generalized regression neural network, and adaptive neuro-fuzzy inference system (ANFIS) to predict the unconfined compressive strength of silty soil. The results indicated that the performance indexes of the AI models are better than the nonlinear regression [46]. Next, the GEP was employed to formulate the unconfined compressive strength with high accuracy [47]. Then, the GEP was utilized to predict the peak ground acceleration [48]. In order to model the peak ground acceleration, artificial neural network (ANN) was suggested. They found that the ANN technique outperformed to the regression method [49]. In addition, AI techniques have been successfully applied for other areas, e.g., ANN [50–55], fuzzy logic [56–59], and ANFIS [60–62]. On the contrary, ANFIS techniques attract much attention because it can accurately formulate a pseudo-fitness function and constraint functions. In order to model the highly nonlinear performances of the 2-DOF compliant mechanism, the ANFIS approach is chosen in this study.

After formulating the approximate models for fitness functions and constraint functions, an optimization method is employed. Until now, a few optimization approaches have been proposed to simultaneously solve the MOO, e.g., desirability [63], gray [64], and Taguchi-combined fuzzy (TCF) [65]. Most of methods are still valuable but the optimal value may trap a local point. Besides, meta-heuristic algorithms have been attracted much attention in MOOs, e.g., genetic algorithm (GA) [66], particle swarm optimization (PSO) [67, 68], differential evolution (DE) [69], improved differential evolution (IDE) [70], cuckoo search algorithm (CSA) [71], improved binary differential evolution algorithm (IBDE) [72], nondominated sorting genetic algorithm II (NSGA-II) [38], interactive Search algorithm (ISA) [73], bi-objective evolutionary algorithm (BOEA) [74], and other algorithms [75–78]. However, the aforementioned algorithms are quite complicated and require a long computing time because they depend on specific-tuned parameters. If unsuitable parameters are used, the optimal solution is not true. In other words, those algorithms limit to optimization problems with multiple constraints. Hence, researchers developed recent algorithms such as teaching learning-based optimization algorithm (TLBO) [79–81], Jaya algorithm [82], and lightning attachment procedure optimization (LAPO) algorithm [83]. These three algorithms have good

behaviors but LAPO can be considered as the best one. So, the LAPO is selected to extend for the 2-DOF compliant mechanism.

From this perspective, this study suggests some new contributions as: (1) A large nonlinear deformation of compliant mechanisms can be resolved by nonlinear FEM. (2) The suggested computational intelligence method is capable of making new populations for evolutionary algorithm. (3) The output performances of the 2-DOF mechanism are changed into a single objective function (SOF) by combination of desirability and fuzzy logic. (4) The SOF is modeled by ANFIS. The output of ANFIS is a pseudo-fitness function which is then optimized by LAPO. (5) The suggested method is hybrid combination of intelligent computation, statistics, FEM, ANFIS, and evolutionary algorithms thanks to its robustness and simplicity. (6) The suggested computational intelligence approach can reach a global optimum value.

The goal of the present paper is to suggest a computational intelligence method which is employed for 2-DOF compliant mechanism. The structure of this article includes following parts. The computational intelligence method is presented in Sect. 2. The optimization formulation for 2-DOF compliant mechanism is described in Sect. 3. Section 4 includes results and discussion. Comparison is given in Section 5. Conclusions and future work are made in Section 6.

2 Computational intelligence method

A computational intelligence method is developed to resolve the MOO process of compliant mechanism in this paper. In the field of precise engineering systems, the 2-DOF compliant mechanism simultaneously needs a large displacement and a small parasitic motion [84]. The suggested computational intelligence method undergoes following phases: (1) mechanical structure, (2) desirability's calculation for objective functions, (3) combination of all objective functions into a single fitness function by fuzzy logic system, (4) modeling the combined fitness function through ANFIS, and (5) maximizing this objective by LAPO algorithm. Figure 1 illustrates the main computational procedure of the suggested method.

Step 1: Design and analysis

Design and analysis undergo the main procedures as follows.

- *Architecture design* This mechanism desires to reach a large displacement and a small parasitic error but it must work under an elastic area of material. The displacement is a performance along the desired axis (e.g., x -axis) while the parasitic error motion is an error

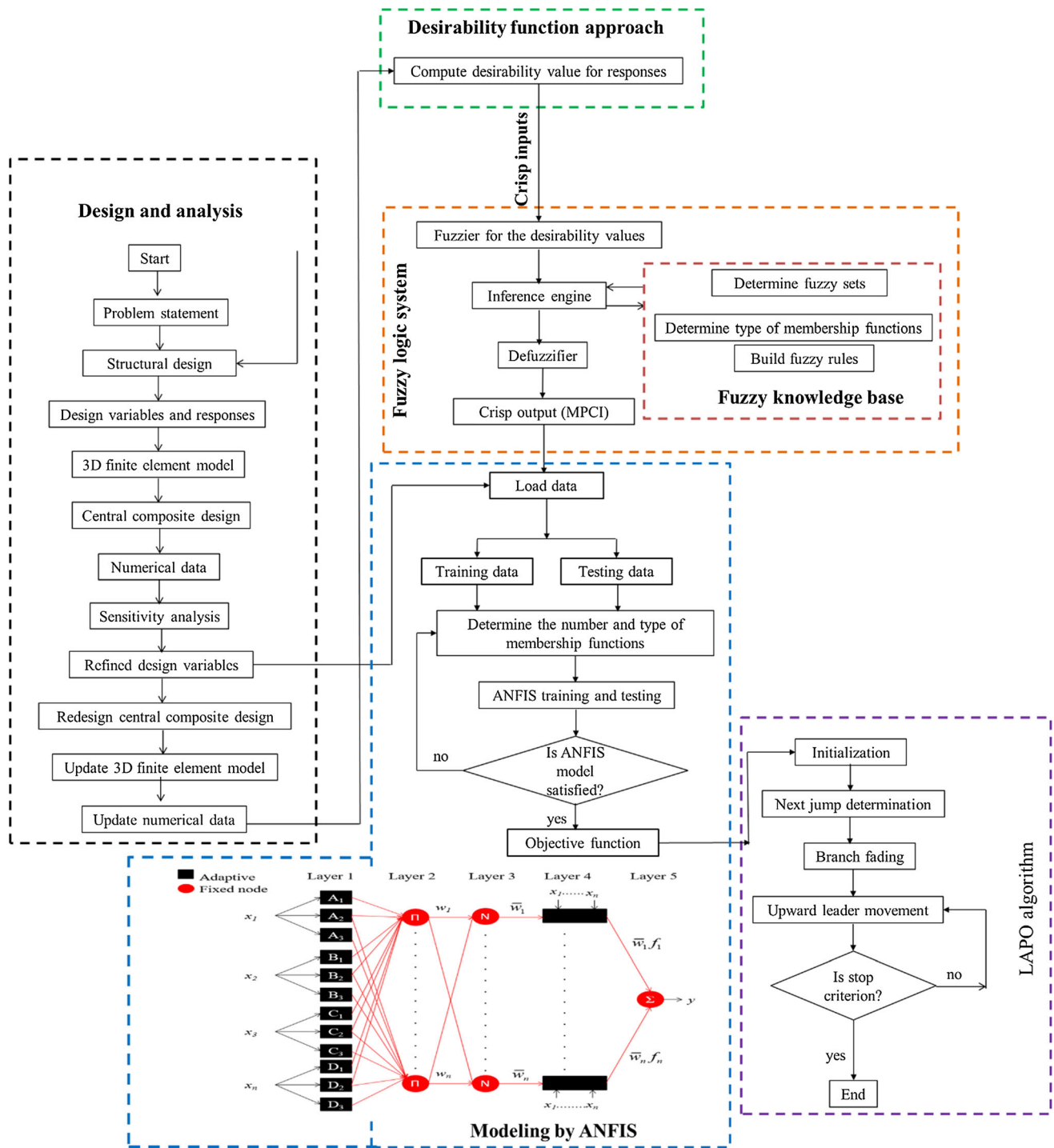


Fig. 1 Suggested framework of computational intelligence method

along the undesired axis (e.g., y-axis). The parasitic motion is perpendicular to the displacement. If parasitic error is limited, and the precision of the mechanism is enhanced.

- *Determination of design variables* This an important task to find the main parameters affecting the performances of the mechanism.

- *Objective functions* The displacement and the parasitic error are the output performances. Particularly, stress is considered as a constraint.
- *Finite element analysis (FEA)* A FEM model is analyzed by FEA implementation to reach the displacement, the parasitic motion, and the equivalent stress (Von Mises stress).

- *Numerical dataset* numerical datasets are got from FEA in which design of experiment is generated by central composite design (CCD).
- *Investigation of sensitivity* It is analyzed by using analysis of variance (ANOVA) and the Taguchi method.
- *Reduce the space of design variables* It helps to find main parameters which contribute to the population space for the LAPO.
- *Rebuild 3D model and recollect numerical dataset* Based on the space of new populations, 3D model is rebuilt, and the corresponding numerical datasets are collected again.

Step 2: Desirability calculation

Step 2 changes the displacement and parasitic error to become the desirability index in a range from zero to one. This helps to avoid a deviation of both performances. The displacement and the parasitic error are suitable with the larger-the-bester and the smaller-the-better, respectively [85].

Larger-the-bester:

$$\begin{cases} D_i = 0, & f^* \leq L_b \\ D_i = \left(\frac{f^* - L_b}{U_b - L_b} \right)^r, & L_b \leq f^* \leq U_b, f^* \text{ is } i\text{th} \\ D_i = 1, & f^* \geq U_b, \end{cases} \tag{1}$$

performance, D_i is desirability value. r is desirability index

Smaller-the-bester:

$$\begin{cases} D_i = 0, f^* \geq U_b \\ D_i = \left(\frac{f^* - U_b}{L_b - U_b} \right)^r, & L_b \leq f^* \leq U_b, \\ D_i = 1, f^* \leq L_b, \end{cases} \tag{2}$$

L_b and U_b are lower and upper range

Step 3: Fuzzy logic modeling

This step is aimed to combine the desirability of displacement and the desirability of parasitic error to become a SOF (see in Fig. 1). A fuzzy logic system [86] is utilized to this modeling process. A decision maker with a support of fuzzy inference system (FIS) and fuzzy if–then rules is employed to the fuzzy output into a non-fuzzy SOF. According to the TCF [65], the SOF is maximized through the Taguchi method to reach the local optimum value. In order to avoid the local optimum value, the SOF is modeled by the ANFIS, and then it is maximized by the LAPO later.

Step 4: ANFIS modeling

ANFIS model [87] is developed model the SOF. The goal of this process is to create the SOF model for the optimization (see in Fig. 1).

Step 5: Optimization by LAPO

LAPO is a recent algorithm in which its basic is replied on a lightning phenomenon [83, 88]. This algorithm is expanded to maximize the SOF in reaching a global optimal design for the suggested 2-DOF mechanism. Details of this algorithm are available in references [83, 88, 89]. Its scheme is given in Fig. 1.

3 Numerical example

A 2-DOF mechanism is studied to confirm the usefulness of the suggested computational intelligence method.

3.1 Optimization formulation for 2-DOF compliant mechanism

A 2-DOF mechanism is created, as in Fig. 2. An actuator (green color) applies a load to a mobile table in the y direction. The output displacement is labeled δ_y . At the same time, the mobile table also makes a parasitic motion in the x -direction (δ_x). In contrast, if a force comes from the actuator in x direction (yellow color), the platform moves in the x -direction while the y -direction movement is a parasitic motion error. The parasitic motion error reduces the positioning precision of the device, which is an undesired motion. Therefore, the displacement should be maximized and the parasitic error is minimized, simultaneously. Overall device is located at four fixed supports by using screws. In general, a change in geometry, material, or configuration can make an expected large

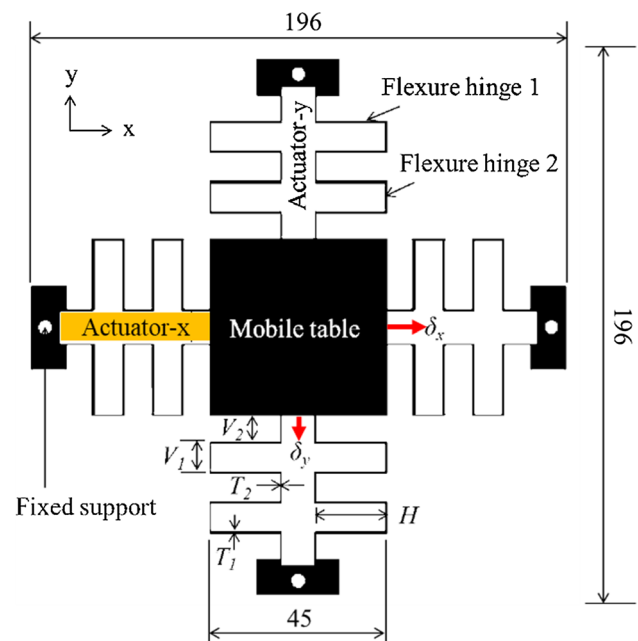


Fig. 2 Diagram of 2-DOF mechanism (unit: mm)

displacement and increase stiffness of undesired motion direction. In this article, we choose stainless steel for material due to its high strength. Besides, leaf springs are adopted for flexure hinges 1 and 2 in order to displace the mobile table because the leaf springs easily fabricate and make a large deformation. As depicted in Fig. 3, the main design parameters consist of a vector of design variable $\mathbf{X} = [V_1, V_2, T_1, T_2, H]^T$. Moreover, the mechanism must work under an allowable stress. Design parameters and of the suggested mechanism are given (see in Table 1). Stainless steel material is utilized for the mechanism with yield stress (σ_Y) of 207 MPa.

According to background of compliant mechanisms [7, 9, 22, 27, 84, 90], the geometrical dimension of flexible hinges is the main design variables which are noted as $\mathbf{X} = [V_1, V_2, T_1, T_2, H]^T$. The objective functions consist of the displacement ($F_1(\mathbf{X})$) and the parasitic error ($F_2(\mathbf{X})$). Stress ($F_3(\mathbf{X})$) is an extra constraint. The optimization for the suggested 2-DOF mechanism is stated as:

$$\text{Find } \mathbf{X} = [T_1, T_2, V_1, V_2, H]^T$$

$$\text{Maximize } F_1(\mathbf{X}) \quad (3)$$

$$\text{Minimize } F_2(\mathbf{X}) \quad (4)$$

Subject to constraint:

$$F_3(\mathbf{X}) \leq \frac{\sigma_Y}{SF}, \text{ SF: Safety factor is chosen as 1.5.} \quad (5)$$

Initial space of design variables:

$$\begin{cases} 0.45 \text{ mm} \leq T_1 \leq 0.65 \text{ mm} \\ 0.5 \text{ mm} \leq T_2 \leq 0.7 \text{ mm} \\ 7 \text{ mm} \leq V_1 \leq 11 \text{ mm} \\ 8 \text{ mm} \leq V_2 \leq 12 \text{ mm} \\ 26 \text{ mm} \leq H \leq 30 \text{ mm} \end{cases} \quad (6)$$

4 Results and discussion

4.1 Setup of simulations

Thickness of the mechanism (w) is 10 mm (see in Fig. 3). Meshing is implemented with fine mesh at the hinges. The meshing quality is well confirmed by Skewness criteria (see in Fig. 4). A load of 15 N exerted the mobile table along the x-axis. The mechanism is fixed by screws at holes. Stainless steel material is also utilized in the simulations.

4.2 Sensitivity analysis of design parameters

The aim of the sensitivity analysis is to estimate which design parameter significantly contributes on the performances of the 2-DOF mechanism. Moreover, the sensitivity evaluation can redetermine the best important design variables which largely influence on the displacement, the parasitic error, and the equivalent stress. The results of this analysis can reduce the searching space of design variables that are utilized for the optimization process later.

As shown in Fig. 2, the geometrical factors (T_1, T_2, V_1, V_2 , and H) are the initial parameters to design the 2-DOF mechanism. Table 2 gives the range of initial parameters. Based on the setup of simulations in Figs. 3 and 4, the initial datasets are collected in Table 3.

The ANOVA analysis for the displacement found that the parameters T_2 and V_2 have very low contributions with 1.06% and 0%, respectively (see in Table 4). Then, Taguchi technique is employed to illustrate the effective plot of design parameters. The results of Taguchi indicated that are two parameters T_2 and V_2 also have smallest influences on the displacement (see in Fig. 5). On the other

Fig. 3 Meshing of the mechanism

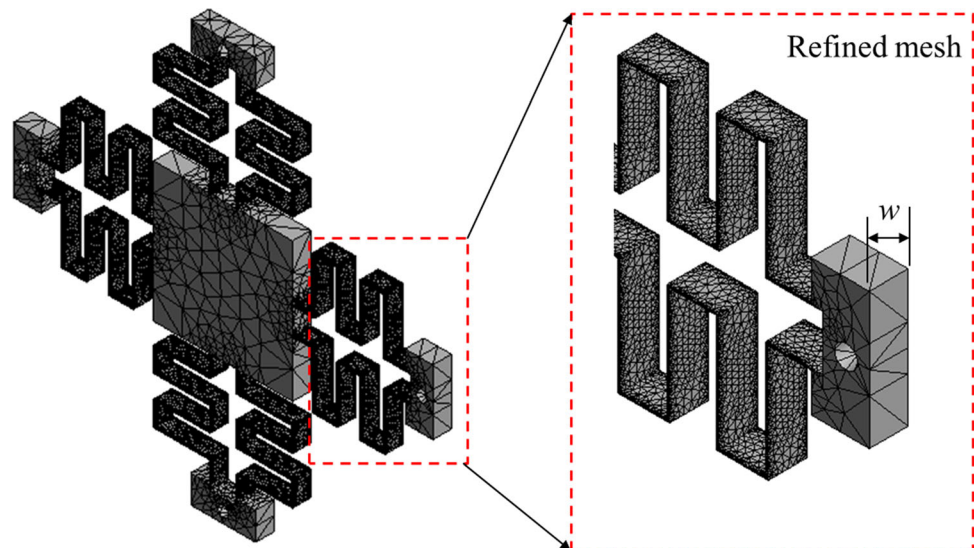


Table 1 Design parameters

Notation	Label	Value
Thickness of flexure hinge 1	T_1	$0.45 \text{ mm} \leq T_1 \leq 0.65 \text{ mm}$
Thickness of flexure hinge 2	T_2	$0.5 \text{ mm} \leq T_2 \leq 0.7 \text{ mm}$
Length of flexure hinge 2	V_1	$7 \text{ mm} \leq V_1 \leq 11 \text{ mm}$
Length of flexure hinge 1	H	$26 \text{ mm} \leq H \leq 30 \text{ mm}$
Distance between mobile table and flexure hinge 1	V_2	$8 \text{ mm} \leq V_2 \leq 12 \text{ mm}$
Total size of the mechanism	S_t	$196 \times 196 \times 10 \text{ mm}^3$
Size of mobile table	S_m	$45 \times 45 \times 10 \text{ mm}^3$
Fixed support by screw	θ	3 mm

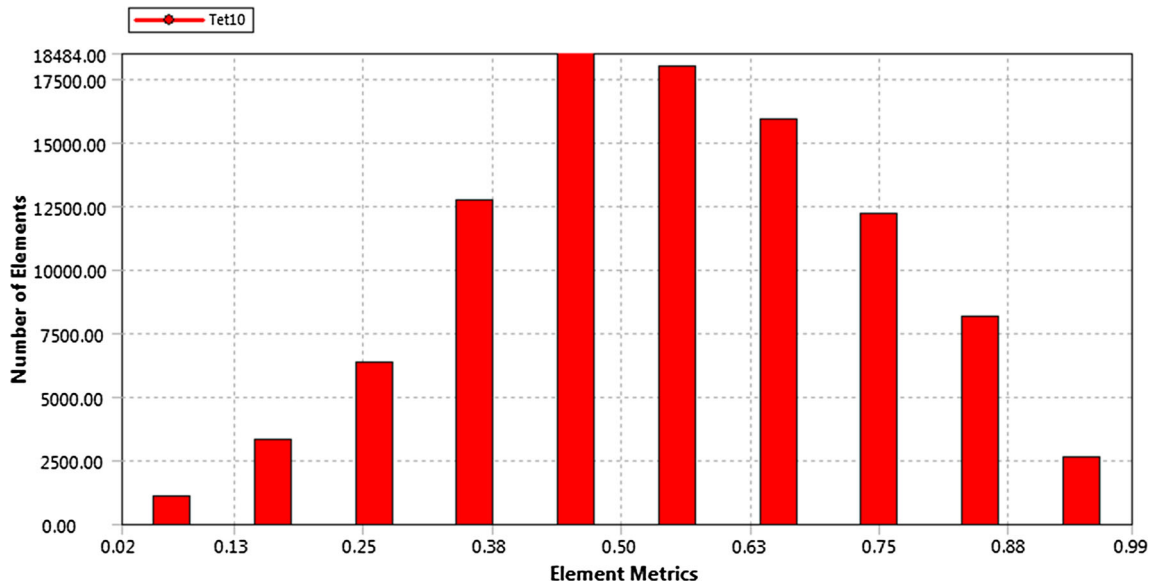


Fig. 4 Meshing quality distribution

Table 2 Overall design parameters

Label	Range (mm)	Value 1	Value 2	Value 3
T_1	$0.45 \leq T_1 \leq 0.65$	0.45	0.55	0.65
T_2	$0.5 \leq T_2 \leq 0.7$	0.5	0.6	0.7
V_1	$7 \leq V_1 \leq 11$	7	9	11
V_2	$8 \leq V_2 \leq 12$	8	10	12
H	$26 \leq H \leq 30$	26	28	30

hand, these two parameters are not significant. They can be abandoned in the modeling and optimizing for the displacement later. Additionally, the results of Table 4 revealed that the p-values of T_2 and V_2 are larger than 0.05. It means that these two factors do not have significant correlation to the displacement. Meanwhile, the p-values of the remaining parameters are smaller than 0.05, and they are significant factors in designing the displacement.

Similarly, the ANOVA is employed for evaluating the parasitic error. The results revealed that the contribution of V_1 is very small with 0.64% to the parasitic error (see in Table 5). The result of Taguchi is the same with the results of ANOVA (see in Fig. 6). Besides, the p-value of V_1 is higher than 0.05. It is noted that this factor has no significant contribution to the parasitic error. Hence, this factor can be abandoned in modeling and optimizing for the parasitic error.

Lastly, the ANOVA results for the stress indicated that the contributions of V_1 and H are very low with 0.19% and 2.26%, respectively (see in in Table 6). From the Taguchi analysis, the results can be concluded the same with the ANOVA results (see in Fig. 7). Moreover, the p-values of these two factors are larger than 0.05. It can conclude that they are not correlated to the stress. So, they can be left from modeling and optimizing for the parasitic error.

Table 3 Initial datasets

Trial	Parameters (mm)						$F_1(\mathbf{X})$ (mm)	$F_2(\mathbf{X})$ (mm)	$F_3(\mathbf{X})$ (MPa)
	T_1	T_2	T_2	V_1	V_2	H			
1	0.55	0.6	9	10	10	28	0.691159546	3.27804553	63.14738
2	0.45	0.6	9	10	10	28	1.48062408	2.068472538	100.0738
3	0.65	0.6	9	10	10	28	0.57487	2.9733	69.619
4	0.55	0.5	9	10	10	28	0.885428905	2.821824835	73.35679
5	0.55	0.7	9	10	10	28	0.5616	3.5636	58.088
6	0.55	0.6	7	10	10	28	0.8087731	2.883451716	71.78896
7	0.55	0.6	11	10	10	28	0.715246618	3.101355104	66.74502
8	0.55	0.6	9	8	8	28	0.838777363	3.183128198	65.03037
9	0.55	0.6	9	12	12	28	0.828020632	2.963956598	69.83908
10	0.55	0.6	9	10	10	26	0.609356463	3.279909061	63.11151
11	0.55	0.6	9	10	10	30	0.865474164	3.018661859	68.57343
12	0.45	0.5	7	8	8	30	1.123795271	2.176007809	95.12834
13	0.65	0.5	7	8	8	26	0.54471	3.112	66.516
14	0.45	0.7	7	8	8	26	0.475849152	3.487027936	59.36287
15	0.65	0.7	7	8	8	30	0.51004	4.7594	43.493
16	0.45	0.5	11	8	8	26	1.037148595	2.451213246	84.44798
17	0.65	0.5	11	8	8	30	1.0683	2.9321	70.597
18	0.45	0.7	11	8	8	30	0.952557325	2.70079298	76.64416
19	0.65	0.7	11	8	8	26	0.40705	3.4713	59.632
20	0.45	0.5	7	12	12	26	1.597374678	2.066197164	100.184
21	0.65	0.5	7	12	12	30	1.0619	2.7151	76.239
22	0.45	0.7	7	12	12	30	1.409378529	2.102362391	98.46067
23	0.65	0.7	7	12	12	26	0.45183	3.578	57.853
24	0.45	0.5	11	12	12	30	2.37579608	1.758489676	117.7147
25	0.65	0.5	11	12	12	26	0.71606	3.1628	65.449
26	0.45	0.7	11	12	12	26	0.844481587	2.313893723	89.4596
27	0.65	0.7	11	12	12	30	0.60898	3.8066	54.379

4.3 Modeling and optimization

4.3.1 Membership function

Table 7 gives the fuzzy labels for f the FIS modeling. The membership function (MFs) for inputs is assigned in Fig. 8a, b. The MFs of the output (SOF) is determined, as depicted in Fig. 9.

4.3.2 Numerical example 1

Numerical example 1 is investigated to show the robustness and efficiency of the developed computation method. Based the results of Table 4 and Fig. 5, whole initial space of design variables is reinitialized to create a new population for the flowing modeling and optimization. Three parameters V_1 , H , and T_1 are the main design parameters. The built SOF is then optimized by LAPO. The optimization for example 1 is presented as.

$$\text{Find } \mathbf{X}_1 = [V_1, H, T_1]^T$$

$$\text{Max SOF}_{\text{numerical example 1}}(\mathbf{X}_1) \tag{7}$$

S.t.

$$\left\{ \begin{array}{l} F_3(\mathbf{X}) \leq \frac{\sigma_y}{SF} \\ 7 \text{ mm} \leq V_1 \leq 11 \text{ mm} \\ 26 \text{ mm} \leq H \leq 30 \text{ mm} \\ 0.45 \text{ mm} \leq T_1 \leq 0.65 \text{ mm} \end{array} \right. \tag{8}$$

The desirability results for the displacement and parasitic error are calculated in Table 8.

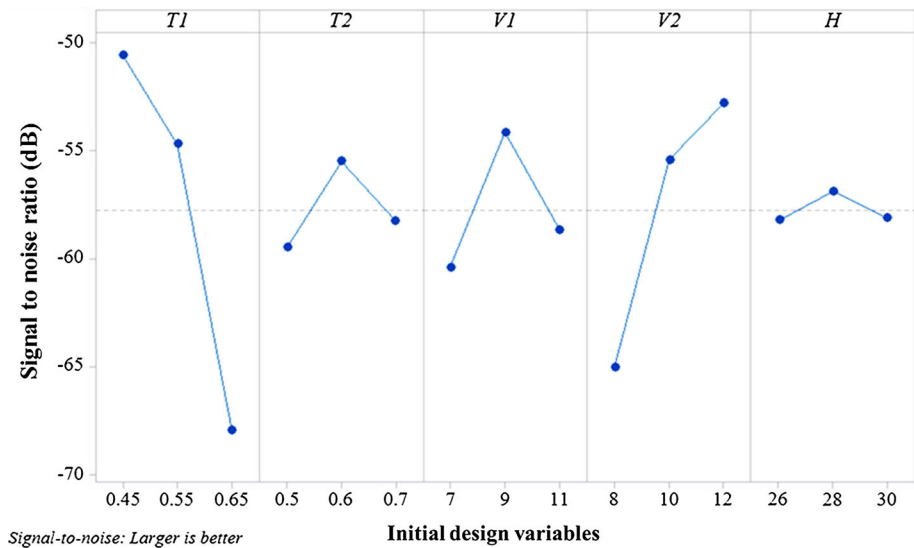
The fuzzy if-then-rules are built for two inputs and one output (SOF), as given in Table 9. These rules are designed according to the designer’s experience. The aim of these rules is to find a correct combination of the D_1 and D_2 values for generating the SOF value.

Next, the FIS implementation is conducted in MATLAB R2019b. The influencing plot among the two inputs and the output is described (see in Fig. 10). Figure 11 illustrates the rules of fuzzy logic modeling.

Table 4 Displacement’s ANOVA

Source	DF	Seq SS	Contribution (%)	Adj SS	Adj MS	F value	p value
Model	20	0.000821	94.79	0.000821	0.000041	5.45	0.022
Linear	5	0.000333	38.49	0.000333	0.000067	8.86	0.010
T_1	1	0.000139	16.02	0.000139	0.000139	18.44	0.005
T_2	1	0.000009	1.06	0.000009	0.000009	1.22	0.311
V_1	1	0.000094	10.89	0.000094	0.000094	12.53	0.012
V_2	1	0.000000	0.00	0.000000	0.000000	0.00	0.994
H	1	0.000091	10.51	0.000091	0.000091	12.10	0.013
Square	5	0.000038	4.39	0.000038	0.000008	1.01	0.484
T_1*T_1	1	0.000008	0.89	0.000001	0.000001	0.15	0.714
T_2*T_2	1	0.000004	0.51	0.000000	0.000000	0.00	0.949
V_1*V_1	1	0.000000	0.00	0.000002	0.000002	0.25	0.638
V_2*V_2	1	0.000003	0.35	0.000000	0.000000	0.05	0.828
$H*H$	1	0.000023	2.64	0.000023	0.000023	3.04	0.132
Two-way interaction	10	0.000450	51.91	0.000450	0.000045	5.97	0.020
T_1*T_2	1	0.000013	1.48	0.000013	0.000013	1.70	0.240
T_1*V_1	1	0.000123	14.24	0.000123	0.000123	16.39	0.007
T_1*V_2	1	0.000012	1.34	0.000012	0.000012	1.54	0.261
T_1*H	1	0.000108	12.49	0.000108	0.000108	14.38	0.009
T_2*V_1	1	0.000017	1.99	0.000017	0.000017	2.29	0.181
T_2*V_2	1	0.000069	7.92	0.000069	0.000069	9.12	0.023
T_2*H	1	0.000003	0.30	0.000003	0.000003	0.35	0.575
V_1*V_2	1	0.000004	0.43	0.000004	0.000004	0.49	0.510
V_1*H	1	0.000071	8.16	0.000071	0.000071	9.39	0.022
V_2*H	1	0.000031	3.55	0.000031	0.000031	4.08	0.090
Error	6	0.000045	5.21	0.000045	0.000008		
Total	26	0.000866	100.00				

Fig. 5 Influencing plot of the displacement



The calculations are proceeded in MATLAB and the results of the SOF value for example 1 are given in Table 10.

Based on a combination of the refined space of design parameters (Table 8) and the calculated SOF value

(Table 10), ANFIS model is built to establish the SOF regression model in relation to the design parameters. In the ANFIS modeling, 70% datasets are for training, 15% datasets are for testing, and 15% datasets for validating.

Table 5 Parasitic error’s ANOVA

Source	DF	Seq SS	Contribution (%)	Adj SS	Adj MS	F value	P value
Model	20	4.64835	96.65	4.64835	0.23242	8.66	0.007
Linear	5	3.67838	76.48	3.67838	0.73568	27.40	0.000
T_1	1	1.59208	33.10	1.59208	1.59208	59.30	0.000
T_2	1	0.97476	20.27	0.97476	0.97476	36.30	0.001
V_1	1	0.03058	0.64	0.03058	0.03058	1.14	0.327
V_2	1	0.47876	9.95	0.47876	0.47876	17.83	0.006
H	1	0.60220	12.52	0.60220	0.60220	22.43	0.003
Square	5	0.26710	5.55	0.26710	0.05342	1.99	0.213
T_1*T_1	1	0.24443	5.08	0.14889	0.14889	5.55	0.057
T_2*T_2	1	0.01258	0.26	0.00806	0.00806	0.30	0.603
V_1*V_1	1	0.00075	0.02	0.00088	0.00088	0.03	0.863
V_2*V_2	1	0.00471	0.10	0.00673	0.00673	0.25	0.635
$H*H$	1	0.00463	0.10	0.00463	0.00463	0.17	0.692
Two-way interaction	10	0.70286	14.61	0.70286	0.07029	2.62	0.126
T_1*T_2	1	0.06744	1.40	0.06744	0.06744	2.51	0.164
T_1*V_1	1	0.00863	0.18	0.00863	0.00863	0.32	0.591
T_1*V_2	1	0.33902	7.05	0.33902	0.33902	12.63	0.012
T_1*H	1	0.03774	0.78	0.03774	0.03774	1.41	0.281
T_2*V_1	1	0.05103	1.06	0.05103	0.05103	1.90	0.217
T_2*V_2	1	0.06350	1.32	0.06350	0.06350	2.37	0.175
T_2*H	1	0.01170	0.24	0.01170	0.01170	0.44	0.534
V_1*V_2	1	0.03860	0.80	0.03860	0.03860	1.44	0.276
V_1*H	1	0.05827	1.21	0.05827	0.05827	2.17	0.191
V_2*H	1	0.02693	0.56	0.02693	0.02693	1.00	0.355
Error	6	0.16110	3.35	0.16110	0.02685		
Total	26	4.80944	100.00				

Fig. 6 Influencing plot of the parasitic error

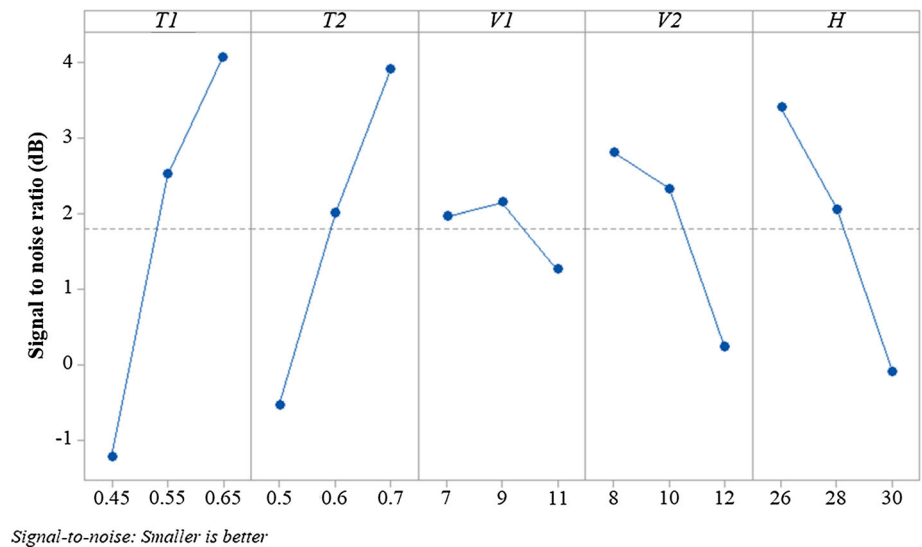


Table 6 Stress’s ANOVA

Source	DF	Seq SS	Contribution (%)	Adj SS	Adj MS	F value	p value
Model	15	6636.90	88.41	6636.90	442.46	5.60	0.003
Linear	5	5817.74	77.50	5817.74	1163.55	14.72	0.000
T_1	1	3689.38	49.15	3689.38	3689.38	46.66	0.000
T_2	1	1287.96	17.16	1287.96	1287.96	16.29	0.002
V_1	1	14.30	0.19	14.30	14.30	0.18	0.679
V_2	1	656.75	8.75	656.75	656.75	8.31	0.015
H	1	169.36	2.26	169.36	169.36	2.14	0.171
Two-way interaction	10	819.16	10.91	819.16	81.92	1.04	0.474
$T_1 * T_2$	1	6.38	0.08	6.38	6.38	0.08	0.782
$T_1 * V_1$	1	5.26	0.07	5.26	5.26	0.07	0.801
$T_1 * V_2$	1	366.28	4.88	366.28	366.28	4.63	0.054
$T_1 * H$	1	219.30	2.92	219.30	219.30	2.77	0.124
$T_2 * V_1$	1	27.05	0.36	27.05	27.05	0.34	0.570
$T_2 * V_2$	1	20.53	0.27	20.53	20.53	0.26	0.620
$T_2 * H$	1	82.87	1.10	82.87	82.87	1.05	0.328
$V_1 * V_2$	1	66.24	0.88	66.24	66.24	0.84	0.380
$V_1 * H$	1	5.13	0.07	5.13	5.13	0.06	0.804
$V_2 * H$	1	20.12	0.27	20.12	20.12	0.25	0.624
Error	11	869.75	11.59	869.75	79.07		
Total	26	7506.65	100.00				

Fig. 7 Influencing plot of the stress

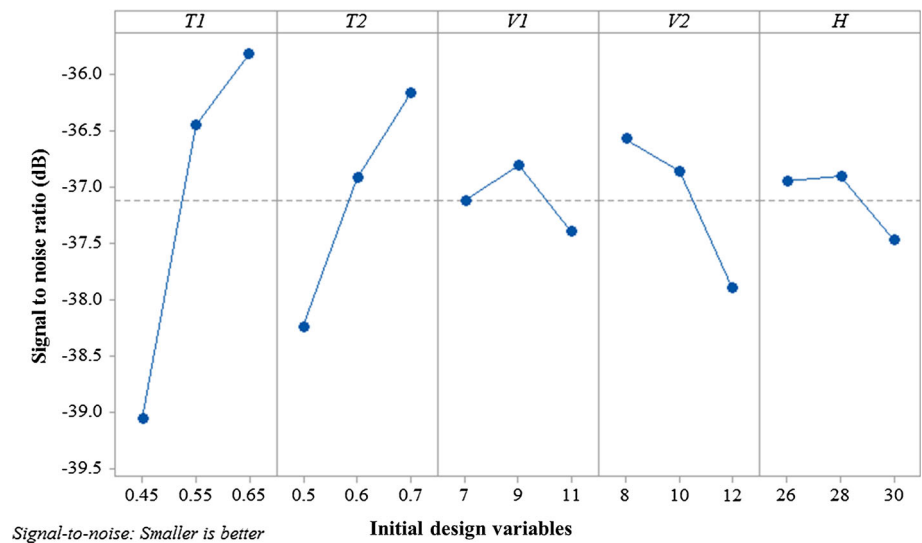


Table 7 Fuzzy labels

Label	VT	VL	NL	L	A	AH	H	VH	VVH
Fuzzy	Very very tiny	Very low	Near low	Low	Average	Average high	High	Very high	Very Very high

And then, MAPE, RMSE, R^2 , and MSE are used to verify the accuracy of the ANFIS predictor [91–94].

$$MAPE = \frac{100\%}{N} \sum_{i=1}^n \left| \frac{z_i - z'_i}{z_i} \right|, \tag{9}$$

Mean absolute percentage error

Fig. 8 MFs for: **a** the desirability of displacement, **b** desirability of parasitic error

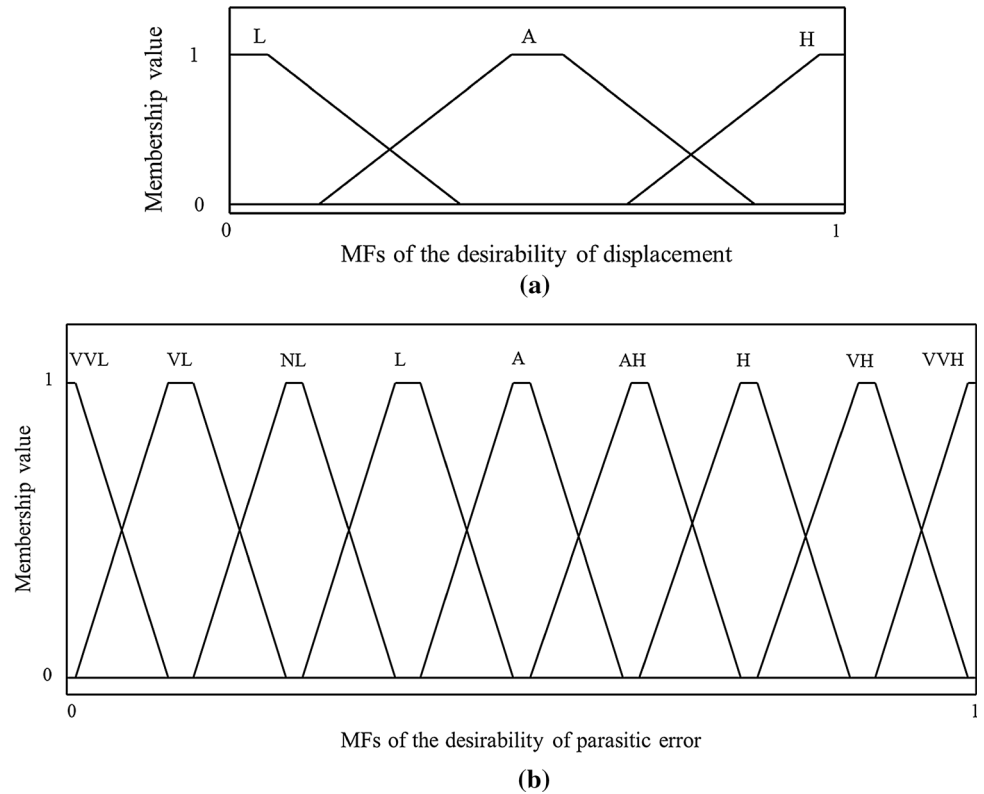
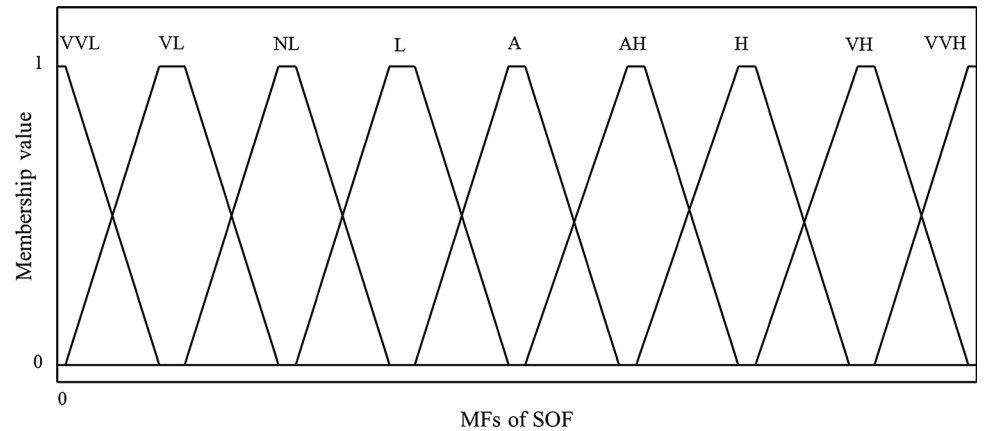


Fig. 9 MFs for the SOF



$$RMSE = \sqrt{\frac{1}{N} \sum_{i=1}^N (z_i - z'_i)^2}, \quad \text{Root mean square error} \quad (10)$$

$$R^2 = 1 - \frac{\sum_{i=1}^N (z_i - z'_i)^2}{\sum_{i=1}^N (z_i - \bar{z}_i)^2}, \quad \text{Correlation coefficient} \quad (11)$$

$$MSE = \frac{1}{N} \sum_{i=1}^N (z_i - z'_i)^2, \quad \text{mean square error} \quad (12)$$

in which z_i is the i th actual value, z'_i is the i th predicted value, and \bar{z} is the average value, and N is number of repetitions.

The results found that the ANFIS parameters include nodes of 78, linear factors of 108, nonlinear factors of 27, total factor of 135, training data of 15, testing data of 5, and fuzzy if-then rules of 27. Besides, the performance indexes are relatively good.

By using the TCF method, the optimal parameters are with $V_1 = 9$ mm, $T_1 = 0.5$ mm, and $H = 28$ mm. The displacement is about 0.911678 mm and the parasitic error is 0.0009359 mm. These optimum points are local optima

Table 8 Numerical results of example 1

Trial	Parameters (Unit: mm)			$F_1(\mathbf{X})$ (mm)	$F_2(\mathbf{X})$ (mm)	$F_3(\mathbf{X})$ (MPa)	Desirability for $F_1(\mathbf{X})$	Desirability for $F_2(\mathbf{X})$
	V_1	H	T_1				D_1	D_2
1	9	28	0.5	1.07935	0.00058	79.26453	0.59360	0.82443
2	7	28	0.5	0.79764	0.00063	74.20616	0.37095	0.86503
3	11	28	0.5	0.73144	0.00183	71.22364	0.44213	0.70596
4	9	26	0.5	0.94955	6.57E-06	72.83156	0.42801	0.83281
5	9	30	0.5	0.86410	0.00303	72.22312	0.89101	0.62964
6	9	28	0.45	0.80384	0.00152	77.83952	0.65736	0.72772
7	9	28	0.55	0.92922	0.00076	66.94232	0.51837	0.87765
8	7	26	0.45	0.68902	0.00180	80.66029	0.37045	0.92212
9	11	26	0.45	0.75295	0.00028	80.31530	0.16468	0.77127
10	7	30	0.45	1.14026	0.00113	91.67427	0.74677	0.53551
11	11	30	0.45	1.07905	0.00530	87.49335	0.86293	0.15343
12	7	26	0.55	0.689615	0.00092	58.87820	0.18977	0.66559
13	11	26	0.55	0.57780	0.00272	61.51795	0.21596	0.72954
14	7	30	0.55	0.75107	0.00155	70.63687	0.41751	0.87708
15	11	30	0.55	1.12654	0.00011	73.99249	0.76564	0.70980

In which: D_1 is the desirability of displacement, D_2 is the desirability of parasitic error

thanks to this reasoning is strongly influenced by the Taguchi technique (see in Table 11).

On the contrary, LAPO algorithm is extended to reach a global optimum value. From the ANFIS modeling, the SOF is maximized. The optimal parameters determine as $V_1 = 7$ mm, $T_1 = 0.45$ mm, and $H = 26$ mm. The displacement is approximately 0.6890 mm and the parasitic error is about 0.0018 mm. Because the SOF predicted by the LAPO is higher than that by the TCF, it can conclude that the suggested computational intelligence method is superior to the TCF method (see in Table 11).

4.3.3 Numerical example 2

In this example, a new population is generated by the use of the results of Table 5 and Fig. 6. Four parameters T_1 , T_2 , V_2 , and H are the main design parameters. The optimization for the example 2 is formulated as.

$$\text{Find } \mathbf{X}_2 = [T_1, T_2, V_2, H]^T$$

$$\text{Max SOF}_{\text{numericaexample2}}(\mathbf{X}_2) \tag{13}$$

S.t.

$$\begin{cases} F_3(\mathbf{X}) \leq \frac{\sigma_y}{SF} \\ 0.45 \text{ mm} \leq T_1 \leq 0.65 \text{ mm} \\ 0.5 \text{ mm} \leq T_2 \leq 0.7 \text{ mm} \\ 8 \text{ mm} \leq V_2 \leq 12 \text{ mm} \\ 26 \text{ mm} \leq H \leq 30 \text{ mm} \end{cases} \tag{14}$$

The desirability values for the displacement and the parasitic error are computed in Table 12.

The results of SOF for example 2 are calculated, as given in Table 13.

By combination of the refined parameters (Table 12) and the SOF (Table 13), ANFIS model is built to establish the SOF model. The ANFIS model incudes nodes of 193, linear factors of 405, nonlinear factors of 36, total factors of 441, training data of 25, testing data of 8, and fuzzy if-then rules of 81. The performance indexes of the established ANFIS model are relatively good.

The optimal parameters are $T_1 = 0.45$ mm, $T_2 = 0.5$ mm, $V_2 = 12$ mm, and $H = 30$ mm based on the TCF approach (Table 14). Using the TCF, the displacement is found about 2.0433 mm and the parasitic error is approximately 0.0047 mm. Through LAPO algorithm, the parameters are found as $T_1 = 0.45$ mm, $T_2 = 0.7$ mm, $V_2 = 12$ mm, and $H = 30$ mm. The displacement is 0.9773 mm and the parasitic error is 0.0105 mm. The predicted SOF by the present method has an efficiency better than the TCF method.

4.3.4 Numerical example 3

From the results of Table 6 and Fig. 7, three main design parameters include T_1 , T_2 , and V_2 . The optimization of numerical example 3 is presented as follows.

$$\text{Find } \mathbf{X}_3 = [T_1, T_2, V_2]^T$$

Table 9 Fuzzy if–then-rules for example 1

Trial	D_1	D_2	SOF
1	L	VLL	VLL
2	A	VLL	VLL
3	H	VLL	VLL
4	L	VL	VL
5	A	VL	VL
6	H	VL	VL
7	L	NL	NL
8	A	NL	NL
9	H	NL	NL
10	L	L	L
11	A	L	L
12	H	L	L
13	L	A	A
14	A	A	A
15	H	A	A
16	L	AH	AH
17	A	AH	AH
18	H	AH	AH
19	L	H	H
20	A	H	H
21	H	H	H
22	L	VH	VH
23	A	VH	VH
24	H	VH	VH
25	L	VVH	VVH
26	A	VVH	VVH
27	H	VVH	VVH

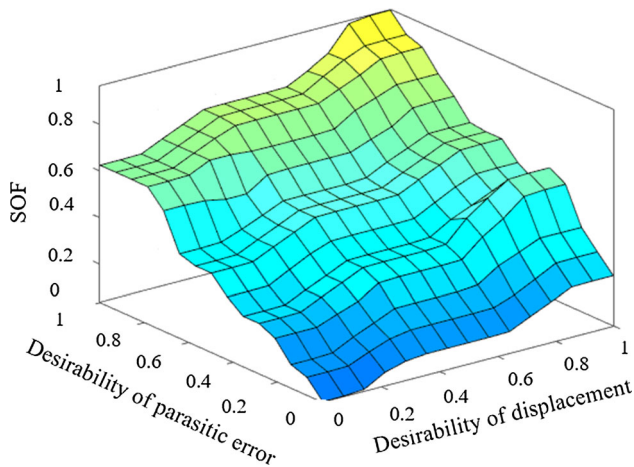


Fig. 10 Influencing plot among inputs and output

$$\begin{aligned} &\text{Max SOF}_{\text{numerical example 3}}(\mathbf{X}_3) \\ &\text{S.t.} \end{aligned} \tag{15}$$

$$\left\{ \begin{aligned} &F_3(\mathbf{X}) \leq \frac{\sigma_y}{SF} \\ &0.45 \text{ mm} \leq T_1 \leq 0.65 \text{ mm} \\ &0.5 \text{ mm} \leq T_2 \leq 0.7 \text{ mm} \\ &8 \text{ mm} \leq V_2 \leq 12 \text{ mm} \end{aligned} \right. \tag{16}$$

The results of desirability are given in Table 15.

The SOF value is calculated, as given in Table 16.

This part builds a relation among the fined parameters (Table 15) and the calculated SOF (Table 16) by establishing ANFIS model. The ANFIS parameters are nodes of 78, linear parameters of 108, nonlinear parameters of 27, total number of parameters of 135, training data of 15, testing data of 5, and fuzzy if–then rules of 27. The performance indexes are calculated with good values for the modeling.

The optimal parameters are $T = 0.45 \text{ mm}$, $T_2 = 0.5 \text{ mm}$, $V_2 = 10 \text{ mm}$ through TCF method (Table 17). The displacement is 1.6126 mm and the parasitic error is 0.0055 mm by the TCF. Then, with the suggested computational method, the optimal parameters are $T_1 = 0.45 \text{ mm}$, $T_2 = 0.5 \text{ mm}$, $V_2 = 12 \text{ mm}$. The results indicated that the displacement is 2.2109 mm and the parasitic error is 0.0028 mm. Additionally, by the present method, the predicted SOF is larger than that of the TCF.

4.4 Discussion

In previous section, a comparison based on the optimum values and the predicted SOF value are not enough. This part carries out an error calculation (E_c) among the forecasted value (V_f) and FEA simulation value (V_s). The comparison results are calculated in Table 18. A relative error is defined as.

$$E_c (\%) = \left| \left(\frac{V_f}{V_s} - 1 \right) * 100 \right| \tag{17}$$

The errors for three numerical examples are approximately 4–6% by using the present method. Meanwhile, the errors are about 68–97%. This confirms that the suggested computational intelligence method is better than the TCF method. The numerical example 3 is the best choose for the mechanism. Overall optimal parameters and performances are given in Table 18.

5 Comparisons

In this part, a few AI methods such as multilayer perceptron (MLP) [46] and deep neural network (DNN) [95] and multiple-linear regression (MLR) [96] are used in comparison with the developed ANFIS model. Three performance indexes (MSE, RMSE, and R^2) in Eqs. (10–12) are

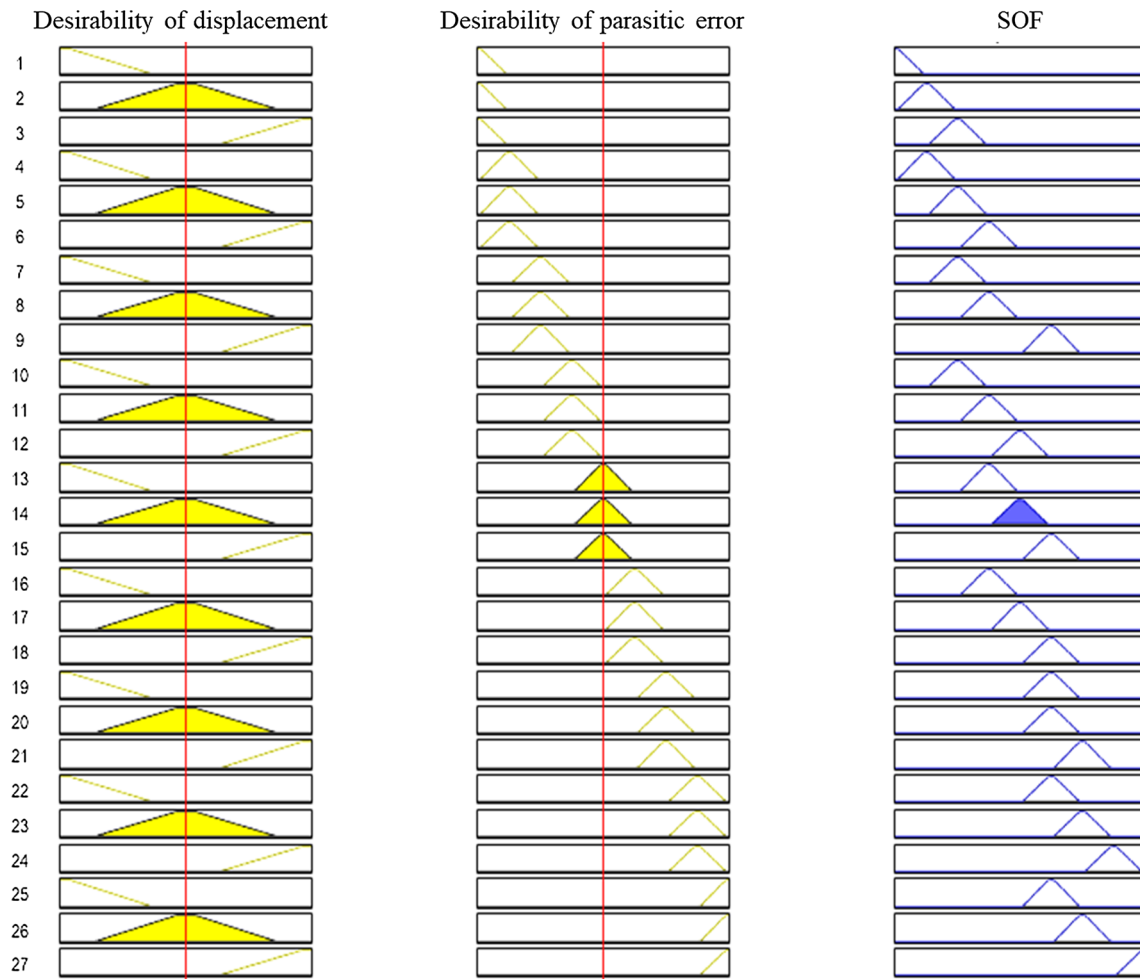


Fig. 11 Suggested fuzzy process

Table 10 Results of SOF for example 1

Trial	D_1	D_2	SOF
1	0.59360	0.82443	0.70
2	0.37095	0.86503	0.75
3	0.44213	0.70596	0.58
4	0.42801	0.83281	0.70
5	0.89101	0.62964	0.62
6	0.65736	0.72772	0.61
7	0.51837	0.87765	0.75
8	0.37045	0.92212	0.75
9	0.16468	0.77127	0.64
10	0.74677	0.53551	0.56
11	0.86293	0.15343	0.43
12	0.18977	0.66559	0.47
13	0.215963	0.729545	0.579
14	0.417519	0.877089	0.75
15	0.765643	0.709807	0.641

employed in this comparison. The MLP and DANN include the same basic parameters as follows: (1) number of hidden layers: 2, (2) number of neurons in each hidden layer: 6, (3) activation function for first hidden layer: rectified linear unit, (4) activation function for first hidden layer: tansig, (5) activation function for output layer: pureline, and (6) training algorithm: Levenberg–Marquardt. The datasets are also divided as same as the proposed ANFIS model, including 70% datasets are for training, 15% datasets are for testing, and 15% datasets for validating. The inputs of datasets include the design parameters and the output is the SOF value. The purpose of modeling is to find the best SOF approximate model before transferring it to the optimization process. As shown in Table 19, the results show that the performance indexes of the proposed ANFIS model (R^2 is close to 1, MSE is around 10^{-4} , and RMSE is about 10^{-2}) are better than those of the MLP, DNN, and MLR. It means that the developed ANFIS model is the reliable and accurate model in

Table 11 Optimal solutions for example 1

Method	Parameters (mm)	Performances		
		Displacement (mm)	Parasitic error (mm)	SOF
TCF	$V_1 = 9$ $H = 28$ $T_1 = 0.5$	$F_1(\mathbf{X}) = 0.9116$	$F_2(\mathbf{X}) = 0.00093$	0.70
Present method	$V_1 = 7$	$F_1(\mathbf{X}) = 0.6890$	$F_2(\mathbf{X}) = 0.00180$	0.75

Table 12 Numerical results of example 2

Trial	Parameters (Unit: mm)				$F_1(\mathbf{X})$ (mm)	$F_2(\mathbf{X})$ (mm)	$F_3(\mathbf{X})$ (MPa)	D_1	D_2
	T_1	T_2	V_2	H					
1	0.55	0.6	10	28	0.69103	0.00245	73.39641	0.24170	0.26721
2	0.45	0.6	10	28	1.25704	0.00963	95.14741	0.48778	0.22041
3	0.65	0.6	10	28	0.75246	0.00084	58.42203	0.21500	0.24705
4	0.55	0.5	10	28	0.87087	0.00227	81.02399	0.33035	0.44270
5	0.55	0.7	10	28	0.54860	0.00178	63.40808	0.05913	0.52202
6	0.55	0.6	8	28	0.65961	0.00958	69.48834	0.12308	0.16378
7	0.55	0.6	12	28	0.81375	0.00124	81.03241	0.29501	0.28620
8	0.55	0.6	10	26	0.60339	0.00252	70.54133	0.19490	0.34857
9	0.55	0.6	10	30	1.06883	0.00116	70.56628	0.32879	0.45674
10	0.45	0.5	8	26	1.10719	0.00052	88.62674	0.38396	0.37146
11	0.65	0.5	8	26	0.54193	0.00052	56.54990	0.09161	0.57368
12	0.45	0.7	8	26	0.49158	0.00279	62.01396	0.07622	0.39730
13	0.65	0.7	8	26	0.32767	0.00061	44.79286	0.06117	0.39607
14	0.45	0.5	12	26	1.68420	0.00055	110.37100	0.72249	0.37772
15	0.65	0.5	12	26	0.69844	4.56E-05	69.24026	0.19751	0.54197
16	0.45	0.7	12	26	0.78741	0.00329	79.80752	0.25723	0.64257
17	0.65	0.7	12	26	0.46378	0.00066	57.26488	0.00955	0.60335
18	0.45	0.5	8	30	1.12031	0.00340	83.21806	0.51550	0.48315
19	0.65	0.5	8	30	0.81465	0.00056	66.69990	0.21763	0.57564
20	0.45	0.7	8	30	0.68455	0.00188	59.94700	0.16102	0.58040
21	0.65	0.7	8	30	0.53622	0.00019	45.57497	0.14045	0.46944
22	0.45	0.5	12	30	2.21093	0.00281	110.45610	0.91098	0.52070
23	0.65	0.5	12	30	0.96381	0.00457	77.14788	0.38048	0.57521
24	0.45	0.7	12	30	0.97728	0.01045	82.19693	0.39898	0.85695
25	0.65	0.7	12	30	0.59823	0.00159	62.25600	0.14578	0.70801

establishing the fitness function for the optimization problem of the 2-DOF compliant mechanism.

Subsequently, the optimal results by the proposed method are compared with the other evolutionary algorithms. The numerical example 3 is a feasibly optimal candidate for the mechanism. In order to confirm the usefulness of the present method, the TLBO [97] and Jaya [98] are integrated with the established ANFIS model for the numerical example 3. Table 20 shows that the estimated displacement and the parasitic error of the present method are better than those of the other methods.

The performances of different methods are continued by the use of nonparametric testing techniques Wilcoxon and

Friedman [67, 99, 100]. A number of 50 simulation runs are for each method. The results show there is difference among the present method with the two other methods thanks to p -value ≤ 0.001 . It can conclude that the present method has a superior behavior compared with other methods (see in Table 21).

The results of Friedman analysis also have the same conclusion in the results of Wilcoxon with to p -value ≤ 0.001 (see in Table 22).

A few advantages of the computational intelligence method for the compliant mechanisms are as follows: The suggested method deals with the global optimal design of the 2-DOF mechanism with a less computational cost.

Table 13 Results of SOF for example 2

Trial	D_1	D_2	SOF
1	0.24170	0.26721	0.30
2	0.48778	0.22041	0.35
3	0.21500	0.24705	0.29
4	0.33035	0.44270	0.42
5	0.05913	0.52202	0.37
6	0.12308	0.16378	0.16
7	0.29501	0.28620	0.33
8	0.19490	0.34857	0.28
9	0.32879	0.45674	0.43
10	0.38396	0.37146	0.37
11	0.09161	0.57368	0.37
12	0.07622	0.39730	0.26
13	0.06117	0.39607	0.26
14	0.72249	0.37772	0.42
15	0.19751	0.54197	0.40
16	0.25723	0.64257	0.50
17	0.00955	0.60335	0.37
18	0.51550	0.48315	0.49
19	0.21763	0.57564	0.42
20	0.16102	0.58040	0.38
21	0.14045	0.46944	0.34
22	0.91098	0.52070	0.62
23	0.38048	0.57521	0.50
24	0.39898	0.85695	0.74
25	0.14578	0.70801	0.53

Table 14 Optimal solutions for example 2

Method	Parameters (mm)	Performances		
		Displacement (mm)	Parasitic error (mm)	SOF
TCF	$T_1 = 0.45$	$F_1(\mathbf{X}) = 2.0433$	$F_2(\mathbf{X}) = 0.0047$	0.60
	$T_2 = 0.5$			
	$V_2 = 12$			
	$H = 30$			
Present method	$T_1 = 0.45$	$F_1(\mathbf{X}) = 0.9773$	$F_2(\mathbf{X}) = 0.0105$	0.73
	$T_2 = 0.7$			
	$V_2 = 12$			
	$H = 30$			

Besides, the present method also some disadvantages include: FEM model becomes more difficult for compliant mechanisms with more complex structures. So, the FEM takes a large computing time. This can be enhanced via using multiple processors. An adaptive dataset with each design stage is out of the goal of the present study, and it can be a future research direction. Furthermore, the AI

techniques can be feasible approaches to become a new design method for compliant mechanisms. However, the AI methods should be only utilized for highly nonlinear behaviors. The mentioned analytical methods in the literature are suitable tools to solve for simple structures of compliant mechanisms. For more complicated structures, the present computational method should be taken into consideration. In future work, the fuzzy logic and ANFIS models can be enhanced if the main parameters can be improved better if their main parameters are properly selected before they are utilized for modeling process.

6 Conclusions

In this article, the computational intelligence method has been devised to resolve the optimal design for the 2-DOF mechanism. It is built by a combination of FEM, statistics, artificial intelligence models, and metaheuristic algorithm. A 2-DOF mechanism is a numerical example to confirm the usefulness of the suggested method. Initially numerical datasets are collected by simulations. ANOVA and Taguchi method are employed in evaluating the parameter’s sensitivity. The analyzed results can generate the new range of design parameters. Based on the datasets from the new design spaces, the desirabilities are determined for the displacement and parasitic error. The calculated results of desirabilities are put into the FIS model as two inputs. The output of the FIS model (SOF) related to the fined design parameters is formulated through ANFIS modeling. The modeled SOF is maximized by LAPO. The results found that the numerical example 3 is determined as the best optimal design for the mechanism.

In evaluating the precision of approximate model, a few AI techniques and regression are utilized in comparison with the developed ANFIS model. The datasets of example 3 are divided into the training, testing, and validating sets for modeling and comparing among the AI and MLR methods. The results indicate that the performance measurements of the proposed ANFIS model (R^2 is close to 1, MSE is around 10^{-4} , and RMSE is about 10^{-2}) are better than those of the MLP, DNN, and MLR. Based on the results of by using Wilcoxon and Friedman analysis, the proposed computational intelligence method is more effective than the TCF, ANFIS-integrated TLBO, and ANFIS-integrated Jaya in searching the optimal displacement and parasitic error. The results revealed that the optimal displacement and parasitic error are approximately 2.2109 mm and 0.0028 mm, respectively. In future work, the achieved results can be facilitated to the optimal design for general compliant mechanisms with irregular shapes and complex structures. Some physical prototypes are manufactured to validate the predicted results. Moreover,

Table 15 Numerical results of example 3

Trial	Parameters (Unit: mm)			$F_1(\mathbf{X})$ (mm)	$F_2(\mathbf{X})$ (mm)	$F_3(\mathbf{X})$ (MPa)	D_1	D_2
	T_1	T_2	V_2					
1	0.55	0.6	10	1.26410	0.00269	76.84500	0.34234	0.49844
2	0.45	0.6	10	1.58790	0.01849	101.6900	0.68495	0.47364
3	0.65	0.6	10	0.98778	0.00056	62.24400	0.25879	0.43193
4	0.55	0.5	10	1.14328	0.00377	85.84876	0.45133	0.66606
5	0.55	0.7	10	1.06500	0.00062	73.48100	0.27303	0.48652
6	0.55	0.6	8	0.70051	0.00442	76.43731	0.06799	0.24092
7	0.55	0.6	12	0.95025	0.00538	74.26800	0.32346	0.47601
8	0.45	0.5	8	1.12031	0.00339	83.21806	0.36320	0.51901
9	0.65	0.5	8	0.92413	0.00079	73.08900	0.19935	0.43202
10	0.45	0.7	8	0.96999	0.00572	82.37400	0.24267	0.37913
11	0.65	0.7	8	0.53622	0.00019	45.57497	0.06427	0.25351
12	0.45	0.5	12	2.21093	0.00281	110.45610	0.92419	0.80695
13	0.65	0.5	12	0.94735	0.00275	71.26000	0.25028	0.48725
14	0.45	0.7	12	1.67830	0.01374	107.72	0.702683	0.43856
15	0.65	0.7	12	0.60350	0.00385	54.997	0.014207	0.110915

Table 16 Results of SOF for example 3

Trial	D_1	D_2	SOF
1	0.34234	0.49844	0.48
2	0.68495	0.47364	0.50
3	0.25879	0.43193	0.38
4	0.45133	0.66606	0.53
5	0.27303	0.48652	0.44
6	0.06799	0.24092	0.25
7	0.32346	0.47601	0.44
8	0.36320	0.51901	0.50
9	0.19935	0.43202	0.34
10	0.24267	0.37913	0.30
11	0.06427	0.25351	0.25
12	0.92419	0.80695	0.80
13	0.25028	0.48725	0.43
14	0.70268	0.43856	0.47
15	0.01420	0.11091	0.12

Table 17 Optimal solutions for example 3

Method	Parameters (mm)	Performances		
		Displacement (mm)	Parasitic error (mm)	SOF
TCF	$T_1 = 0.45$ $T_2 = 0.5$ $V_2 = 10$	$F_1(\mathbf{X}) = 1.6126$	$F_2(\mathbf{X}) = 0.0055$	0.70
Present method	$T_1 = 0.45$ $T_2 = 0.5$ $V_2 = 12$	$F_1(\mathbf{X}) = 2.2109$	$F_2(\mathbf{X}) = 0.0028$	0.80

Table 18 Summary of feasible candidates

Numerical example	Method	Parameters (mm)	Performances		
			$F_1(\mathbf{X})$ (mm)	$F_2(\mathbf{X})$ (mm)	SOF
Numerical example 1	TCF	$V_1 = 9$	$V_f = 0.9116$	$V_f = 0.0009$	0.70
		$H = 28$	$V_s = 0.7660$	$V_s = 0.0029$	
		$T_1 = 0.5$	$E_c = 19\%$	$E_c = 68.36\%$	
	Present method	$V_1 = 7$	$V_f = 0.6890$	$V_f = 0.0018$	0.75
$H = 26$		$V_s = 0.7199$	$V_s = 0.0017$		
$T_1 = 0.45$		$E_c = 4.3\%$	$E_c = 4.4\%$		
Numerical example 2	TCF	$T_1 = 0.45$	$V_f = 2.0433$	$V_f = 0.0047$	0.60
		$T_2 = 0.5$	$V_s = 1.7053$	$V_s = 0.0110$	
		$V_2 = 12$	$E_c = 97.46\%$	$E_c = 56.64\%$	
	Present method	$T_1 = 0.45$	$V_f = 0.9773$	$V_f = 0.0105$	0.73
		$T_2 = 0.7$	$V_s = 1.0096$	$V_s = 0.0110$	
		$V_2 = 12$	$E_c = 3.19\%$	$E_c = 5.05\%$	
Numerical example 3	TCF	$T_1 = 0.45$	$V_f = 1.61269$	$V_f = 0.0055$	0.70
		$T_2 = 0.5$	$V_s = 1.7265$	$V_s = 0.0005$	
		$V_2 = 10$	$E_c = 6.59\%$	$E_c = 855\%$	
	Present method	$T_1 = 0.45$	$V_f = 2.2109$	$V_f = 0.0028$	0.80

Table 19 Comparison among approximate models

Method	Performance index	Model	Training	Testing	Validating
MLP	MSE	0.0038	0.0003	0.005	0.0212
	RMSE	0.0616	0.0173	0.0707	0.1456
	R^2	0.8385	0.9748	0.8068	0.7264
DNN	MSE	0.0096	0.0093	0.0480	0.0232
	RMSE	0.0980	0.0964	0.2191	0.1523
	R^2	0.8840	0.9803	0.8150	0.8233
MLR	MSE	0.0063	0.0035	0.0032	0.0012
	RMSE	0.0794	0.0592	0.0566	0.0346
	R^2	0.7293	0.7668	0.7735	0.7942
Proposed ANFIS	MSE	0.00012	0.00016	0.00015	0.00013
	RMSE	0.0110	0.0126	0.0122	0.0114
	R^2	0.9997	1	0.9885	0.9796

Table 20 Feasible candidates by different methods

Methods	$F_1(\mathbf{X})$ (mm)	$F_2(\mathbf{X})$ (mm)
ANFIS-integrated TLBO ($T_1 = 0.63$ mm, $T_2 = 0.51$ mm, $V_2 = 10.5$ mm)	1.5671	0.0081
ANFIS-integrated Jaya ($T_1 = 0.5$ mm, $T_2 = 0.63$ mm, $V_2 = 10.8$ mm)	1.6093	0.0029
Present method ($T_1 = 0.45$ mm, $T_2 = 0.5$ mm, $V_2 = 12$ mm)	2.2109	0.0028

Table 21 Wilcoxon results

Wilcoxon statistic	<i>p</i> value	Difference
Wilcoxon for $F_1(\mathbf{X})$		
Present method compared with ANFIS-integrated TLBO		
0.0	≤ 0.001	– 0.6438
Present method compared with ANFIS-integrated Jaya		
0.0	≤ 0.001	– 0.6016
Wilcoxon for $F_2(\mathbf{X})$		
Present method compared with ANFIS-integrated TLBO		
1275	≤ 0.001	0.0053
Present method compared with ANFIS-integrated Jaya		
1275	≤ 0.001	0.0001

Table 22 Friedman results

Method	Median	Sum of ranks
Friedman for $F_1(\mathbf{X})$		
ANFIS-integrated Jaya	1.60930	100
ANFIS-integrated TLBO	1.56710	50
Present method	2.21090	150
Overall	1.79577	
<i>p</i> value	≤ 0.001	
Friedman for $F_2(\mathbf{X})$		
ANFIS-integrated Jaya	0.0029	100
ANFIS-integrated TLBO	0.0081	150
Present method	0.0028	50
Overall	0.0046	
<i>p</i> value	≤ 0.001	

the main controllable parameters of the AI methods can be optimized to find the best suitable factors for modeling.

Acknowledgements This research is funded by Vietnam National Foundation for Science and Technology Development (NAFOSTED) under Grant Number 107.01-2019.14.

Compliance with ethical standards

Conflict of interest The authors declare that they have no conflict of interest.

References

- Hao G, Kong X (2012) A novel large-range XY compliant parallel manipulator with enhanced out-of-plane stiffness. *J Mech Des Trans ASME*. <https://doi.org/10.1115/1.4006653>
- Hao G (2017) Determinate synthesis of symmetrical, monolithic tip-tilt-piston flexure stages. *J Mech Des Trans ASME*. <https://doi.org/10.1115/1.4035965>
- Choi K, Lee JJ, Kim GH et al (2018) Amplification ratio analysis of a bridge-type mechanical amplification mechanism based on a fully compliant model. *Mech Mach Theory* 121:355–372. <https://doi.org/10.1016/j.mechmachtheory.2017.11.002>
- Parvari Rad F, Verthey R, Berselli G, Parenti-Castelli V (2016) Analytical compliance analysis and finite element verification of spherical flexure hinges for spatial compliant mechanisms. *Mech Mach Theory* 101:168–180. <https://doi.org/10.1016/j.mechmachtheory.2016.01.010>
- Qingsong X (2015) Design of asymmetric flexible micro-gripper mechanism based on flexure hinges. *Adv Mech Eng* 7:1–8. <https://doi.org/10.1177/1687814015590331>
- Hao G (2018) A framework of designing compliant mechanisms with nonlinear stiffness characteristics. *Microsyst Technol*. <https://doi.org/10.1007/s00542-017-3538-y>
- Hao G, Dai F, He X, Liu Y (2017) Design and analytical analysis of a large-range tri-symmetrical 2R1T compliant mechanism. *Microsyst Technol* 23:4359–4366
- Riza M, Hao G (2019) A flexure motion stage system for light beam control. *Microsyst Technol*. <https://doi.org/10.1007/s00542-018-4168-8>
- Tran NT, Le Chau N, Dao TP (2020) A new butterfly-inspired compliant joint with 3-DOF in-plane motion. *Arab J Sci Eng*. <https://doi.org/10.1007/s13369-020-04415-8>
- Wang Y, Luo Z, Zhang X, Kang Z (2014) Topological design of compliant smart structures with embedded movable actuators. *Smart Mater Struct*. <https://doi.org/10.1088/0964-1726/23/4/045024>
- Ling M, Cao J, Zeng M et al (2016) Enhanced mathematical modeling of the displacement amplification ratio for piezoelectric compliant mechanisms. *Smart Mater Struct* 25:1–11. <https://doi.org/10.1088/0964-1726/25/7/075022>
- Cao J, Ling M, Inman DJ, Lin J (2016) Generalized constitutive equations for piezo-actuated compliant mechanism. *Smart Mater Struct* 25:1–10. <https://doi.org/10.1088/0964-1726/25/9/095005>
- Hansen BJ, Carron CJ, Jensen BD et al (2007) Plastic latching accelerometer based on bistable compliant mechanisms. *Smart Mater Struct*. <https://doi.org/10.1088/0964-1726/16/5/055>
- Chau NL, Tran NT, Dao T (2020) Design and Performance Analysis of a TLET-Type Flexure Hinge. *Adv Mater Sci Eng*. <https://doi.org/10.1155/2020/8293509>
- Howell LL, Midha A (1994) A method for the design of compliant mechanisms with small-length flexural pivots. *J Mech Des Trans ASME* 116:280–290. <https://doi.org/10.1115/1.2919359>
- Valentini PP, Cirelli M, Pennestrì E (2019) Second-order approximation pseudo-rigid model of flexure hinge with parabolic variable thickness. *Mech Mach Theory*. <https://doi.org/10.1016/j.mechmachtheory.2019.03.006>
- Verotti M (2020) A pseudo-rigid body model based on finite displacements and strain energy. *Mech Mach Theory* 149:103811. <https://doi.org/10.1016/j.mechmachtheory.2020.103811>
- Wang N, Zhang Z, Zhang X (2019) Stiffness analysis of corrugated flexure beam using stiffness matrix method. *Proc Inst Mech Eng Part C J Mech Eng Sci* 233:1818–1827. <https://doi.org/10.1177/0954406218772002>
- Chen S, Ling M, Zhang X (2018) Design and experiment of a millimeter-range and high-frequency compliant mechanism with two output ports. *Mech Mach Theory* 126:201–209. <https://doi.org/10.1016/j.mechmachtheory.2018.04.003>
- Teo TJ, Chen IM, Yang G, Lin W (2010) A generic approximation model for analyzing large nonlinear deflection of beam-based flexure joints. *Precis Eng* 34:607–618. <https://doi.org/10.1016/j.precisioneng.2010.03.003>
- Ling M, Howell LL, Cao J, Chen G (2020) Kinetostatic and dynamic modeling of flexure-based compliant mechanisms: a survey. *Appl Mech Rev*. <https://doi.org/10.1115/1.4045679>

22. Lobontiu N (2002) Compliant mechanisms: design of flexure hinges. CRC Press, Boca Raton
23. Le ZhuW, Zhu Z, Guo P, Ju BF (2018) A novel hybrid actuation mechanism based XY nanopositioning stage with totally decoupled kinematics. *Mech Syst Signal Process* 99:747–759. <https://doi.org/10.1016/j.ymsp.2017.07.010>
24. Le ZhuW, Zhu Z, Shi Y et al (2016) Design, modeling, analysis and testing of a novel piezo-actuated XY compliant mechanism for large workspace nano-positioning. *Smart Mater Struct* 25:1–17. <https://doi.org/10.1088/0964-1726/25/1/115033>
25. Hao G, Kong X (2013) A normalization-based approach to the mobility analysis of spatial compliant multi-beam modules. *Mech Mach Theory*. <https://doi.org/10.1016/j.mechmachtheory.2012.08.013>
26. Hao G, Yu J (2016) Design, modelling and analysis of a completely-decoupled XY compliant parallel manipulator. *Mech Mach Theory* 102:179–195
27. Hao G, Li H (2016) Extended static modeling and analysis of compliant compound parallelogram mechanisms considering the initial internal axial force. *J Mech Robot*. <https://doi.org/10.1115/1.4032592>
28. Hao G, Li H (2015) Conceptual designs of multi-degree of freedom compliant parallel manipulators composed of wire-beam based compliant mechanisms. *Proc Inst Mech Eng Part C J Mech Eng Sci*. <https://doi.org/10.1177/0954406214535925>
29. Friedrich R, Lammering R, Rösner M (2014) On the modeling of flexure hinge mechanisms with finite beam elements of variable cross section. *Precis Eng* 38:915–920. <https://doi.org/10.1016/j.precisioneng.2014.06.001>
30. Albanesi AE, Pucheta MA, Fachinotti VD (2013) A new method to design compliant mechanisms based on the inverse beam finite element model. *Mech Mach Theory*. <https://doi.org/10.1016/j.mechmachtheory.2013.02.009>
31. Alkayem NF, Cao M, Zhang Y et al (2018) Structural damage detection using finite element model updating with evolutionary algorithms: a survey. *Neural Comput Appl* 30:389–411
32. Zhu B, Zhang X, Wang N (2013) Topology optimization of hinge-free compliant mechanisms with multiple outputs using level set method. *Struct Multidiscip Optim* 47:659–672. <https://doi.org/10.1007/s00158-012-0841-1>
33. Wang N, Zhang Z, Zhang X, Cui C (2018) Optimization of a 2-DOF micro-positioning stage using corrugated flexure units. *Mech Mach Theory* 121:683–696. <https://doi.org/10.1016/j.mechmachtheory.2017.11.021>
34. Liu M, Zhang X, Fatikow S (2016) Design and analysis of a high-accuracy flexure hinge. *Rev Sci Instrum*. <https://doi.org/10.1063/1.4948924>
35. Xu Q, Li Y (2011) Analytical modeling, optimization and testing of a compound bridge-type compliant displacement amplifier. *Mech Mach Theory* 46:183–200. <https://doi.org/10.1016/j.mechmachtheory.2010.09.007>
36. Dao TP, Huang SC (2017) Design and multi-objective optimization for a broad self-amplified 2-DOF monolithic mechanism. *Sadhana Acad Proc Eng Sci* 42:1527–1542. <https://doi.org/10.1007/s12046-017-0714-9>
37. Choi KB, Han CS (2007) Optimal design of a compliant mechanism with circular notch flexure hinges. *Proc Inst Mech Eng Part C J Mech Eng Sci* 221:385–392. <https://doi.org/10.1243/0954406JMES312>
38. Fossati GG, Miguel LFF, Casas WJP (2019) Multi-objective optimization of the suspension system parameters of a full vehicle model. *Optim Eng* 20:151–177. <https://doi.org/10.1007/s11081-018-9403-8>
39. Arasu MV, Arokiyaraj S, Viayaraghavan P et al (2019) One step green synthesis of larvicidal, and azo dye degrading antibacterial nanoparticles by response surface methodology. *J Photochem Photobiol B Biol* 190:154–162. <https://doi.org/10.1016/j.jphotochem.2018.11.020>
40. Wang CY, Zhang YQ, Zhao WZ (2018) Multi-objective optimization of a steering system considering steering modality. *Adv Eng Softw* 126:61–74. <https://doi.org/10.1016/j.advengsoft.2018.09.012>
41. Güllü H, Fedakar Hİ (2017) Response surface methodology for optimization of stabilizer dosage rates of marginal sand stabilized with Sludge Ash and fiber based on UCS performances. *KSCE J Civ Eng*. <https://doi.org/10.1007/s12205-016-0724-x>
42. Jiang P, Wang C, Zhou Q et al (2016) Optimization of laser welding process parameters of stainless steel 316L using FEM, Kriging and NSGA-II. *Adv Eng Softw* 99:147–160. <https://doi.org/10.1016/j.advengsoft.2016.06.006>
43. Güllü H (2013) On the prediction of shear wave velocity at local site of strong ground motion stations: an application using artificial intelligence. *Bull Earthq Eng*. <https://doi.org/10.1007/s10518-013-9425-8>
44. Güllü H (2017) A new prediction method for the rheological behavior of grout with bottom ash for jet grouting columns. *Soils Found*. <https://doi.org/10.1016/j.sandf.2017.05.006>
45. Güllü H (2017) A novel approach to prediction of rheological characteristics of jet grout cement mixtures via genetic expression programming. *Neural Comput Appl*. <https://doi.org/10.1007/s00521-016-2360-2>
46. Güllü H, Fedakar Hİ (2017) On the prediction of unconfined compressive strength of silty soil stabilized with bottom ash, jute and steel fibers via artificial intelligence. *Geomech Eng* 12:441–464. <https://doi.org/10.12989/gae.2017.12.3.441>
47. Güllü H (2014) Function finding via genetic expression programming for strength and elastic properties of clay treated with bottom ash. *Eng Appl Artif Intell*. <https://doi.org/10.1016/j.engappai.2014.06.020>
48. Güllü H (2012) Prediction of peak ground acceleration by genetic expression programming and regression: a comparison using likelihood-based measure. *Eng Geol*. <https://doi.org/10.1016/j.enggeo.2012.05.010>
49. Güllü H, Erçelebi E (2007) A neural network approach for attenuation relationships: an application using strong ground motion data from Turkey. *Eng Geol*. <https://doi.org/10.1016/j.enggeo.2007.05.004>
50. Wang B, Moayedi H, Nguyen H et al (2019) Feasibility of a novel predictive technique based on artificial neural network optimized with particle swarm optimization estimating pullout bearing capacity of helical piles. *Eng Comput*. <https://doi.org/10.1007/s00366-019-00764-7>
51. Koopialipoor M, Fahimifar A, Ghaleini EN et al (2019) Development of a new hybrid ANN for solving a geotechnical problem related to tunnel boring machine performance. *Eng Comput*. <https://doi.org/10.1007/s00366-019-00701-8>
52. Macura L, Voznak M (2017) Multi-criteria analysis and prediction of network incidents using monitoring system. *J Adv Eng Comput* 1:29. <https://doi.org/10.25073/jaec.201711.47>
53. Wong EWC, Kim DK (2018) A simplified method to predict fatigue damage of TTR subjected to short-term VIV using artificial neural network. *Adv Eng Softw* 126:100–109. <https://doi.org/10.1016/j.advengsoft.2018.09.011>
54. Li Z, Shi K, Dey N et al (2017) Rule-based back propagation neural networks for various precision rough set presented KANSEI knowledge prediction: a case study on shoe product form features extraction. *Neural Comput Appl*. <https://doi.org/10.1007/s00521-016-2707-8>
55. Talaat M, Gobran MH, Wasfi M (2018) A hybrid model of an artificial neural network with thermodynamic model for system diagnosis of electrical power plant gas turbine. *Eng Appl Artif Intell*. <https://doi.org/10.1016/j.engappai.2017.10.014>

56. Ahmed SS, Dey N, Ashour AS et al (2017) Effect of fuzzy partitioning in Crohn's disease classification: a neuro-fuzzy-based approach. *Med Biol Eng Comput*. <https://doi.org/10.1007/s11517-016-1508-7>
57. Ngan TT, Tuan TM, Son LH et al (2016) Decision making based on fuzzy aggregation operators for medical diagnosis from dental X-ray images. *J Med Syst*. <https://doi.org/10.1007/s10916-016-0634-y>
58. Mhetre NA, Deshpande AV, Mahalle PN (2016) Trust management model based on fuzzy approach for ubiquitous computing. *Int J Ambient Comput Intell*. <https://doi.org/10.4018/IJACI.2016070102>
59. Bandyopadhyay S, Das S, Datta A (2020) A hybrid fuzzy filtering—fuzzy thresholding technique for region of interest detection in noisy images. *Appl Intell*. <https://doi.org/10.1007/s10489-019-01551-z>
60. Moayedi H, Raftari M, Sharifi A et al (2019) Optimization of ANFIS with GA and PSO estimating α ratio in driven piles. *Eng Comput*. <https://doi.org/10.1007/s00366-018-00694-w>
61. Sreedhara BM, Rao M, Mandal S (2018) Application of an evolutionary technique (PSO–SVM) and ANFIS in clear-water scour depth prediction around bridge piers. *Neural Comput Appl* 6:1–15. <https://doi.org/10.1007/s00521-018-3570-6>
62. Le Chau N, Dao TP, Dang VA (2019) An efficient hybrid approach of improved adaptive neural fuzzy inference system and teaching learning-based optimization for design optimization of a jet pump-based thermoacoustic-stirling heat engine. *Neural Comput Appl*. <https://doi.org/10.1007/s00521-019-04249-y>
63. Costa NR, Lourenço J, Pereira ZL (2011) Desirability function approach: a review and performance evaluation in adverse conditions. *Chemom Intell Lab Syst* 107:234–244. <https://doi.org/10.1016/j.chemolab.2011.04.004>
64. Huang SC, Dao TP (2016) Multi-objective optimal design of a 2-DOF flexure-based mechanism using hybrid approach of grey-Taguchi coupled response surface methodology and entropy measurement. *Arab J Sci Eng* 41:5215–5231. <https://doi.org/10.1007/s13369-016-2242-z>
65. Dao T-P (2016) Multiresponse optimization of a compliant guiding mechanism using hybrid Taguchi-grey based fuzzy logic approach. *Math Probl Eng*. <https://doi.org/10.1155/2016/5386893>
66. Keshtiar M, Golabi S, Tarkesh Esfahani R (2019) Multi-objective optimization of stainless steel 304 tube laser forming process using GA. *Eng Comput*. <https://doi.org/10.1007/s00366-019-00814-0>
67. Chau NL, Le HG, Dao T et al (2019) Efficient hybrid method of FEA-based RSM and PSO algorithm for multi-objective optimization design for a compliant rotary joint for upper limb assistive device. *Math Probl Eng*. <https://doi.org/10.1155/2019/2587373>
68. Ding S, Du W, Zhao X et al (2019) A new asynchronous reinforcement learning algorithm based on improved parallel PSO. *Appl Intell*. <https://doi.org/10.1007/s10489-019-01487-4>
69. Dao T-P, Huang S-C, Le Chau N (2017) Robust parameter design for a compliant microgripper based on hybrid Taguchi-differential evolution algorithm. *Microsyst Technol*. <https://doi.org/10.1007/s00542-017-3534-2>
70. Ha MH, Vu QV, Truong VH (2020) Optimization of nonlinear inelastic steel frames considering panel zones. *Adv Eng Softw* 142:102771. <https://doi.org/10.1016/j.advengsoft.2020.102771>
71. Dao T-P, Huang S-C, Thang PT (2017) Hybrid Taguchi-cuckoo search algorithm for optimization of a compliant focus positioning platform. *Appl Soft Comput J*. <https://doi.org/10.1016/j.asoc.2017.04.038>
72. Qian S, Ye Y, Liu Y, Xu G (2018) An improved binary differential evolution algorithm for optimizing PWM control laws of power inverters. *Optim Eng* 19:271–296. <https://doi.org/10.1007/s11081-017-9354-5>
73. Mortazavi A, Toğan V, Moloodpoor M (2019) Solution of structural and mathematical optimization problems using a new hybrid swarm intelligence optimization algorithm. *Adv Eng Softw* 127:106–123. <https://doi.org/10.1016/j.advengsoft.2018.11.004>
74. Hsieh TJ (2020) Data-driven oriented optimization of resource allocation in the forging process using bi-objective evolutionary algorithm. *Eng Appl Artif Intell*. <https://doi.org/10.1016/j.engappai.2019.103469>
75. Senkerik R, Zelinka I, Pluhacek M (2017) Chaos-based optimization—a review. *J Adv Eng Comput* 1:68. <https://doi.org/10.25073/jaec.201711.1.51>
76. Zatloukal F, Znoj J (2017) Malware detection based on multiple PE headers identification and optimization for specific types of files. *J Adv Eng Comput* 1:153. <https://doi.org/10.25073/jaec.201712.64>
77. Chernogorov I, Polyakh V, Yarakhmedov O (2017) Search optimization opportunities of modified self-organizing migrating algorithm in multi-extremal tasks environment. *J Adv Eng Comput* 1:144. <https://doi.org/10.25073/jaec.201712.60>
78. Dinh-Cong D, Pham-Duy S, Nguyen-Thoi T (2018) Damage detection of 2D frame structures using incomplete measurements by optimization procedure and model reduction. *J Adv Eng Comput* 2:164. <https://doi.org/10.25073/jaec.201823.203>
79. Venkata Rao R (2016) Review of applications of TLBO algorithm and a tutorial for beginners to solve the unconstrained and constrained optimization problems. *Decis Sci Lett* 5:1–30. <https://doi.org/10.5267/j.dsl.2015.9.003>
80. Nenavath H, Jatoh RK (2018) Hybrid SCA–TLBO: a novel optimization algorithm for global optimization and visual tracking. *Neural Comput Appl* 6:1–30. <https://doi.org/10.1007/s00521-018-3376-6>
81. Niknam T, Azizpanah-Abarghoee R, Rasoul Narimani M (2012) A new multi objective optimization approach based on TLBO for location of automatic voltage regulators in distribution systems. *Eng Appl Artif Intell*. <https://doi.org/10.1016/j.engappai.2012.07.004>
82. Rao RV, Keesari HS, Oclon P, Taler J (2019) An adaptive multi-team perturbation-guiding Jaya algorithm for optimization and its applications. *Eng Comput*. <https://doi.org/10.1007/s00366-019-00706-3>
83. Nematollahi AF, Rahiminejad A, Vahidi B (2017) A novel physical based meta-heuristic optimization method known as lightning attachment procedure optimization. *Appl Soft Comput J* 59:596–621. <https://doi.org/10.1016/j.asoc.2017.06.033>
84. Howell LL, Magleby SP, Olsen BM (2013) Handbook of compliant mechanisms. Wiley, Hoboken
85. Derringer G, Suich R (1980) Simultaneous optimization of several response variables. *J Qual Technol* 12:214–219. <https://doi.org/10.1080/00224065.1980.11980968>
86. Díaz-Cortés MA, Cuevas E, Gálvez J, Camarena O (2017) A new metaheuristic optimization methodology based on fuzzy logic. *Appl Soft Comput J* 61:549–569. <https://doi.org/10.1016/j.asoc.2017.08.038>
87. Zhou J, Li C, Arslan CA et al (2019) Performance evaluation of hybrid FFA-ANFIS and GA-ANFIS models to predict particle size distribution of a muck-pile after blasting. *Eng Comput*. <https://doi.org/10.1007/s00366-019-00822-0>
88. Foroughi Nematollahi A, Rahiminejad A, Vahidi B (2019) A novel multi-objective optimization algorithm based on lightning attachment procedure optimization algorithm. *Appl Soft Comput J* 75:404–427. <https://doi.org/10.1016/j.asoc.2018.11.032>

89. Zheng T, Luo W (2019) An enhanced lightning attachment procedure optimization with quasi-opposition-based learning and dimensional search strategies. *Comput Intell Neurosci* 2019:1–24. <https://doi.org/10.1155/2019/1589303>
90. Howell LL, Midha A (1996) A loop-closure theory for the analysis and synthesis of compliant mechanisms. *J Mech Des Trans ASME*. <https://doi.org/10.1155/1.2826842>
91. Roshani GH, Karami A, Nazemi E (2019) An intelligent integrated approach of Jaya optimization algorithm and neuro-fuzzy network to model the stratified three-phase flow of gas–oil–water. *Comput Appl Math*. <https://doi.org/10.1007/s40314-019-0772-1>
92. Nhu VH, Hoang ND, Duong VB et al (2019) A hybrid computational intelligence approach for predicting soil shear strength for urban housing construction: a case study at Vinhomes Imperia project, Hai Phong city (Vietnam). *Eng Comput*. <https://doi.org/10.1007/s00366-019-00718-z>
93. Shang Y, Nguyen H, Bui XN et al (2019) A novel artificial intelligence approach to predict blast-induced ground vibration in open-pit mines based on the firefly algorithm and artificial neural network. *Nat Resour Res*. <https://doi.org/10.1007/s11053-019-09503-7>
94. Dao T-P, Huang S-C (2015) Design, fabrication, and predictive model of a 1-dof translational flexible bearing for high precision mechanism. *Trans Can Soc Mech Eng* 39:419–429
95. Kumar Y, Dubey AK, Arora RR, Rocha A (2020) Multiclass classification of nutrients deficiency of apple using deep neural network. *Neural Comput Appl*. <https://doi.org/10.1007/s00521-020-05310-x>
96. Ge Y, Wu H (2020) Prediction of corn price fluctuation based on multiple linear regression analysis model under big data. *Neural Comput Appl*. <https://doi.org/10.1007/s00521-018-03970-4>
97. Rao RV, Savsani VJ, Vakharia DP (2011) Teaching-learning-based optimization: a novel method for constrained mechanical design optimization problems. *CAD Comput Aided Des* 43:303–315. <https://doi.org/10.1016/j.cad.2010.12.015>
98. Rao RV, Rai DP, Ramkumar J, Balic J (2016) A new multi-objective Jaya algorithm for optimization of modern machining processes. *Adv Prod Eng Manag*. <https://doi.org/10.14743/apem2016.4.226>
99. Li LM, Di LuK, Zeng GQ et al (2016) A novel real-coded population-based extremal optimization algorithm with polynomial mutation: a non-parametric statistical study on continuous optimization problems. *Neurocomputing*. <https://doi.org/10.1016/j.neucom.2015.09.075>
100. García S, Molina D, Lozano M, Herrera F (2009) A study on the use of non-parametric tests for analyzing the evolutionary algorithms' behaviour: a case study on the CEC'2005 special session on real parameter optimization. *J Heuristics* 15:617–644. <https://doi.org/10.1007/s10732-008-9080-4>

Publisher's Note Springer Nature remains neutral with regard to jurisdictional claims in published maps and institutional affiliations.